

Modelled and measured concentrations of peroxy radicals and nitrate radical in the U.S. Gulf Coast region during TexAQS 2006

Roberto Sommariva · Tim S. Bates · Daniel Bon · Daniel M. Brookes · Joost A. de Gouw · Jessica B. Gilman · Scott C. Herndon · William C. Kuster · Brian M. Lerner · Paul S. Monks · Hans D. Osthoff · Alex E. Parker · James M. Roberts · Sara C. Tucker · Carsten Warneke · Eric J. Williams · Mark S. Zahniser · Steven S. Brown

Received: 26 August 2011 / Accepted: 26 March 2012
© Springer Science+Business Media B.V. 2012

Abstract Measurements of total peroxy radicals ($\text{HO}_2 + \text{RO}_2$) and nitrate radical (NO_3) were made on the NOAA research vessel R/V *Brown* along the U.S. Gulf Coast during the TexAQS 2006 field campaign. The measurements were modelled using a constrained box-model based upon the Master Chemical Mechanism (MCM). The agreement between modelled and measured $\text{HO}_2 + \text{RO}_2$ was typically within ~40% and, in the unpolluted regions, within 30%. The analysis of the model results suggests that the MCM might underestimate the concentrations of some acyl peroxy radicals and other small peroxy radicals. The model underestimated the measurements of NO_3 by 60–70%, possibly because of rapid heterogeneous uptake of N_2O_5 . The MCM model results were used to estimate the composition of the peroxy radical pool and to quantify the role of DMS, isoprene and alkenes in the formation of RO_2 in the different regions. The measurements of $\text{HO}_2 + \text{RO}_2$ and NO_3 were also used to calculate the gas-phase budget of NO_3 and quantify the

R. Sommariva (✉) · D. Bon · J. A. de Gouw · J. B. Gilman · W. C. Kuster · B. M. Lerner · H. D. Osthoff · J. M. Roberts · S. C. Tucker · C. Warneke · E. J. Williams · S. S. Brown
Earth System Research Laboratory, NOAA, Boulder, CO, USA
e-mail: r.sommariva@uea.ac.uk

R. Sommariva · D. Bon · J. A. de Gouw · J. B. Gilman · W. C. Kuster · B. M. Lerner · H. D. Osthoff · S. C. Tucker · C. Warneke · E. J. Williams
CIRES, University of Colorado, Boulder, CO, USA

T. S. Bates
Pacific Marine Environmental Laboratory, NOAA, Seattle, WA, USA

D. M. Brookes · P. S. Monks · A. E. Parker
Department of Chemistry, University of Leicester, Leicester, UK

S. C. Herndon · M. S. Zahniser
Aerodyne Research, Inc., Billerica, MA, USA

importance of organic peroxy radicals as NO_3 sinks. RO_2 accounted, on average, for 12–28% of the total gas-phase NO_3 losses in the unpolluted regions and for 1–2% of the total gas-phase NO_3 losses in the polluted regions.

Keywords Peroxy radicals · RO_2 · Nitrate radical · NO_3 · MCM · TexAQS 2006

1 Introduction

The concentrations and reactivities of radical species, such as OH, NO_3 and peroxy radicals, are central to our understanding of atmospheric chemical processes. Peroxy radicals are intermediates in the oxidation of Volatile Organic Compounds (VOCs), which is mostly initiated by OH during the day and, in polluted areas, by NO_3 during the night. Ozone (O_3) and other radicals, such as halogen atoms (e.g., Cl) also contribute to the oxidation of VOCs and to the formation of peroxy radicals. Except for HO_2 , peroxy radicals are organic compounds (RO_2), whose number and structures depend on the concentrations of the precursor VOCs and on the fragmentation patterns created by their reactions with NO, HO_2 and other organic peroxy radicals. Typically, the most common organic peroxy radical is CH_3O_2 , but the composition of the RO_2 pool can be very complex and it largely depends on the mixture of VOCs in an air mass, which in turn depends on the history of the air mass itself.

The importance of peroxy radicals is mainly related to the conversion of NO to NO_2 , which drives the photochemical formation of ozone in the troposphere, via the photolysis of NO_2 (Monks 2005). Additionally, previous studies (Mihelcic et al. 1993; Canosa-Mas et al. 1996; Carslaw et al. 1997; Salisbury et al. 2001; Geyer et al. 2003; Vaughan et al. 2006; Sommariva et al. 2009) have indicated that organic peroxy radicals interact with the nitrate radical (NO_3) and that, under certain conditions,

Present Address:

R. Sommariva
School of Environmental Sciences, University of East Anglia, Norwich, UK

Present Address:

D. Bon
Department of Civil & Environmental Engineering, Washington State University,
Pullman, WA, USA

Present Address:

D. M. Brookes
Air Quality Practice, AEA plc., Harwell, Didcot, UK

Present Address:

H. D. Osthoff
Department of Chemistry, University of Calgary, Calgary, AB, Canada

Present Address:

A. E. Parker
PC2A, Université des Sciences et Technologies de Lille, Lille, France

Present Address:

S. C. Tucker
Ball Aerospace & Technologies Corp., Boulder, CO, USA

the $\text{RO}_2 + \text{NO}_3$ reactions can be significant sinks for NO_3 , generate OH at night and decrease night-time loss of NO_x species, thus affecting the photochemical formation of ozone at sunrise. The composition of the peroxy radical pool is important to understand the relationship of peroxy radicals chemistry to the nitrogen, HO_x ($\text{OH} + \text{HO}_2$) and ozone budgets. In this work, measurements of total peroxy radicals ($\text{HO}_2 + \text{RO}_2$) and NO_3 were analyzed using a highly detailed chemical box-model based upon the Master Chemical Mechanism (MCM, Saunders et al. 2003, Jenkin et al. 2003).

The measurements were taken during the Texas Air Quality Study (TexAQS) 2006 field campaign onboard the NOAA research vessel *R/V Brown*. The TexAQS 2006 cruise took place between July 27th and September 11th 2006, with the objective to study air quality in the U.S. Gulf Coast region and in the Houston, Texas, area. The *R/V Brown* sailed from Charleston, South Carolina, to Houston, Texas, along the Gulf coast, in the Galveston Bay and in the Houston Ship Channel (Fig. 1). A variety of air masses were sampled during the cruise, ranging from clean marine air sampled off the coast of Florida and in the Gulf of Mexico to polluted air sampled in the industrial areas of the Gulf Coast region. The study area (Fig. 1) and its characteristics have been described in a previous paper (Sommariva et al. 2011), which also details the observations of $\text{HO}_2 + \text{RO}_2$ made during the *R/V Brown* cruise, as well as in other related papers (Parrish et al. 2009; Gilman et al. 2009; Tucker et al. 2010).

The main objective of this paper is to assess the agreement between the model and the measurements of $\text{HO}_2 + \text{RO}_2$ and NO_3 as an indicator of our understanding of radical chemistry under a variety of conditions. Simultaneous in-situ observations of $\text{HO}_2 + \text{RO}_2$ and NO_3 during the cruise make a detailed investigation of the

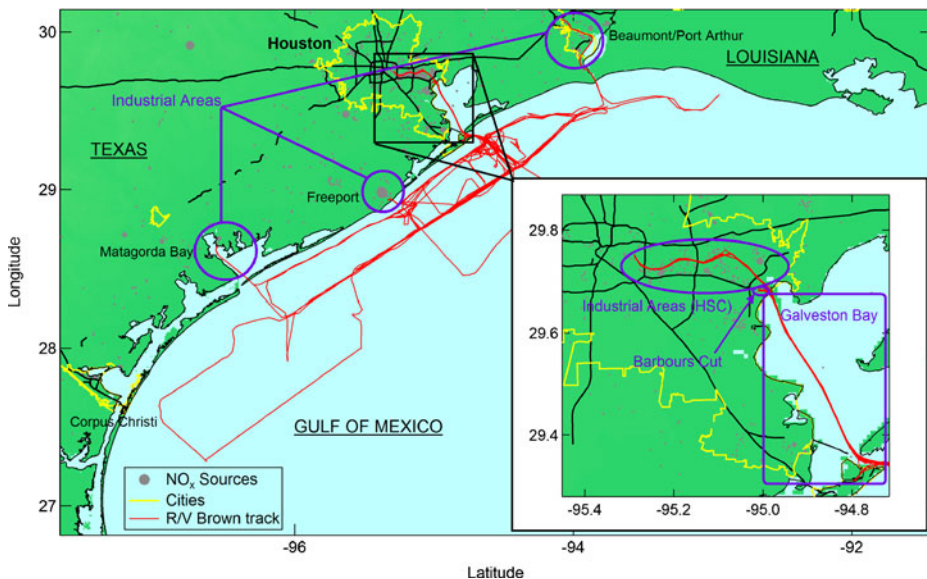


Fig. 1 Cruise of the *R/V Brown* during the Texas Air Quality Study 2006. HSC indicates the Houston Ship Channel

interactions between these radicals possible. The explicit description of the chemistry in the model allowed us to determine the composition of the peroxy radical pool (i.e., which individual peroxy radicals contributed the most to the total $\text{HO}_2 + \text{RO}_2$), how this was related with the composition of an air mass and how it affected radical chemistry in the region. The model construction and assumptions are described in Section 2; the model results are shown and discussed in Sections 3 and 4.

2 Methods

2.1 MCM model

The model was built according to the procedure outlined in Carslaw et al. (1999, 2002), Sommariva et al. (2006, 2009) using a chemical mechanism taken from the Master Chemical Mechanism (MCM) version 3.1 (<http://mcm.leeds.ac.uk/MCMv3.1/>). The MCM is a quasi-explicit chemical mechanism for tropospheric chemistry and contains the detailed degradation processes of 135 VOCs, plus a complete inorganic chemistry mechanism assembled using the IUPAC Gas Kinetic Data Evaluation (Atkinson et al. 2006). The MCM mechanism protocol is described in Jenkin et al. (1997, 2003), Saunders et al. (2003).

In this work a subset of the MCM v3.1 containing 65 VOCs plus CH_4 and CO was used. Dimethyl sulphide (DMS) is not included in version 3.1 of the MCM, so the DMS oxidation mechanism used in previous studies (Carslaw et al. 1999, 2002; Sommariva et al. 2006, 2009) was added to the MCM model. The model was integrated using an off-line version of AtChem (<https://atchem.leeds.ac.uk/webapp/>) and constrained to the measured or estimated values of CO , CH_4 , H_2 , NO , NO_2 , O_3 , SO_2 , H_2O , 65 VOCs, $j(\text{O}^1\text{D})$, $j(\text{NO}_2)$, $j(\text{NO}_3)$, aerosol surface area, temperature, pressure, latitude and longitude. Description and details of the measured parameters and of the instruments can be found in Bates et al. (2008) (aerosol surface area), Parrish et al. (2009) (NO_x , O_3 , SO_2 , H_2O , photolysis rates), Gilman et al. (2009), Warneke et al. (2010) (CO , VOCs).

Methane (CH_4) and molecular hydrogen (H_2) were not measured on the R/V *Brown* during the 2006 cruise. Based on average values measured by the NOAA Global Monitoring Division (<http://www.esrl.noaa.gov/gmd/>) stations close to the area of the TexAQS 2006 cruise a constant value of 520 ppb was used for H_2 ; a constant value of 1800 ppm (open ocean regions) and 1850 ppm (coastal and polluted regions) was used for CH_4 . The Gas Chromatography (GC) method used to measure VOCs (Gilman et al. 2009) could not resolve all the isomers of xylenes and ethyl-methyl-benzenes: the ratio between m-xylene and p-xylene and the ratio between 1-ethyl-3-methyl-benzene and 1-ethyl-4-methyl-benzene were assumed to be 1:1.

To test the sensitivity of the model results to these approximations, the model was run with changed ($\pm 10\%$) methane and molecular hydrogen concentrations. The impact on the species of interest was limited: on average, OH changed by $<2\%$, HO_2 by $<1\%$, CH_3O_2 and CH_3CO_3 by $<6\%$, $\text{C}_2\text{H}_5\text{CO}_3$ by $\sim 5\%$, total organic peroxy radicals (RO_2) by $<2\%$ and NO_3 by $<3\%$. The difference in calculated HO_2 and CH_3O_2 was slightly higher ($\sim 8\text{--}12\%$) in clean marine air than in polluted air, where most of the radical reactivity was controlled by species other than CH_4 , such as oxygenated VOCs and alkenes (Gilman et al. 2009). The ratios of xylenes and

ethyl-methyl-benzenes isomers were also varied, but the radical concentrations did not change in a significant way (<1%).

The model also included dry deposition terms for the appropriate species (O_3 , NO_2 , SO_2 , HNO_3 , H_2O_2 , $HCHO$, CH_3CHO , alkyl nitrates, organic hydroperoxides, organic acids, PANs) as in previous studies (Carslaw et al. 1999, 2002; Sommariva et al. 2006, 2009) and was constrained to the mixing height determined by the NOAA High Resolution Doppler Lidar (HRDL, Tucker et al. 2010) which was onboard the R/V *Brown*. Heterogeneous uptake of 34 gas-phase species was assumed to be irreversible and calculated using Eq. 1 (Fuchs and Sutugin 1970):

$$k_{\text{het}} = \frac{A\bar{c}\gamma}{4} \quad (1)$$

where A is the aerosol surface area ($\text{cm}^2 \text{cm}^{-3}$), \bar{c} is the mean molecular speed of the gas molecule (cm s^{-1}) and γ is the uptake coefficient. The uptake coefficients were taken from Atkinson et al. (2006), except for $\gamma_{N_2O_5}$ which was set to 0.02 (Aldener et al. 2006) and γ_{HO_2} : the value of γ_{HO_2} was set to 0.2 based on the work by Thornton et al. (2008), although this is likely an upper limit value (Thornton and Abbatt 2005). Recent laboratory studies (Taketani et al. 2008, 2009) have reported lower values (0.07–0.19) on sea-salt and sulphate aerosol at 75% relative humidity, but changing γ_{HO_2} to 0.1 did not have a significant impact on modelled $HO_2 + RO_2$. The aerosol surface area was calculated using the aerosol number and size distributions measured on the R/V *Brown* at 60% relative humidity and corrected using a humidity growth factor (Bates et al. 2008).

The model results were compared to the measurements (Sections 3.1, 3.2, 4.1) of total peroxy radicals ($HO_2 + RO_2$) by Peroxy Radical Chemical Amplification (PERCA, Sommariva et al. 2011) and of NO_3 by Cavity Ring-Down Spectroscopy (CaRDS, Dubé et al. 2006). Both instruments were located in a container on the forward upper deck of the R/V *Brown*, about 20 meters above sea level. The $HO_2 + RO_2$ measurements by PERCA had an overall 2- σ uncertainty of 40% with a detection limit of 2 ppt ($= 5.0 \times 10^7 \text{ molecule cm}^{-3}$) for 1 min integration time (Sommariva et al. 2011). The NO_3 measurements by CaRDS had an overall 2- σ uncertainty of 25% with a detection limit of 2 ppt ($= 5.0 \times 10^7 \text{ molecule cm}^{-3}$) for 1 s integration time (Osthoff et al. 2006).

Assessing the uncertainties in the MCM calculation is complex, owing to the very large number of reactions and kinetic parameters involved: Sommariva et al. (2004) estimated the uncertainty of OH as 30–40% and of HO_2 as 25–30% under very clean unpolluted conditions. No estimate was given for CH_3O_2 or other organic peroxy radicals, nor for NO_3 . The MCM model uncertainties are likely greater under polluted conditions due to the larger number of VOCs involved, for many of which the kinetic data in the MCM were estimated owing to lack of laboratory experiments (Jenkin et al. 1997).

2.2 Model results

The model was run for the 30 days of the R/V *Brown* cruise during TexAQS 2006 (July 30th to September 12th, with a 4 days break on August 18th–22nd); the model results were filtered to exclude the periods when one or more of the model constraints were missing (e.g., during calibrations, instrument downtimes, power

failures, sampling of the ship's exhaust) and averaged to have the same frequency of the observations. The results were also filtered to exclude all concentrations lower than twice the reported detection limits of the instruments.

The model calculated the concentrations of all the non-constrained species; modelled OH and $\text{HO}_2/(\text{HO}_2 + \text{RO}_2)$ ratio were used in Sommariva et al. (2011) together with measured $\text{HO}_2 + \text{RO}_2$, NO_x , O_3 and photolysis rates to calculate the in-situ photochemical formation of ozone during TexAQS 2006. In the following sections (Sections 3 and 4) the focus will be on HO_2 , organic peroxy radicals (RO_2) and NO_3 , with the objectives of: (1) assessing how well the model can reproduce the observations, (2) determining the composition of the peroxy radicals pool and (3) investigating the interactions between the nitrate radical and the peroxy radicals.

The modelled results were divided into regions, defined by the location of the R/V *Brown* (Fig. 1, see also Sommariva et al. 2011), with different chemical conditions. Air masses sampled when the R/V *Brown* was in the Atlantic Ocean and in the Gulf of Mexico were classified as either Open Ocean or Gulf Coast, depending on whether they had travelled for a long period of time over the ocean or they were coming from the continent. The distinction was made using the observations of ^{222}Rn —a marker of continental influence—taken onboard the R/V *Brown* (Bates et al. 2008): air masses with low levels of ^{222}Rn ($\leq 500 \text{ mBq/m}^3$) were classified as Open Ocean, while air masses with higher levels of ^{222}Rn were classified as Gulf Coast (Sommariva et al. 2011). The Galveston Bay region (Fig. 1) was characterized by recirculation of air masses from the continent (i.e., more processed air) and heavy traffic of ships and barges. The Industrial Areas included the Houston Ship Channel (HSC) and the Matagorda, Freeport and Beaumont harbours with their concentrations of petrochemical and industrial complexes. Barbours Cut is a shipping dock South of the Houston Ship Channel (Fig. 1): although the chemical composition of the air masses sampled in Barbours Cut was not very different from those in Galveston Bay and in Industrial Areas, these data were analyzed separately, as this was the location where the R/V *Brown* spent the longest period of time during the cruise. The observations and the model results were then averaged to obtain diurnal (i.e., day-time + night-time) profiles in each region.

3 Peroxy radicals ($\text{HO}_2 + \text{RO}_2$)

3.1 Model-measurements comparison for peroxy radicals

The time series of measured and modelled $\text{HO}_2 + \text{RO}_2$ are shown in Fig. 2 and the average diurnal profiles in different regions are shown in Fig. 3. In general, the agreement between the model and the measurements was satisfactory throughout the cruise: the campaign average modelled-to-measured ratio was 0.59, which is within the uncertainty of the measurements (Sommariva et al. 2011). Previous studies with similarly constrained models based upon the MCM showed comparable levels of agreement (typically 30–40% or better) with the measurements for total peroxy radicals, especially under unpolluted or semi-polluted conditions (Carslaw et al. 1999, 1997; Fleming et al. 2006; Emmerson et al. 2007). There were, however, large differences in the model-measurements agreements in different regions and at different times of the day. Figure 3 shows that the model could reproduce the diurnal

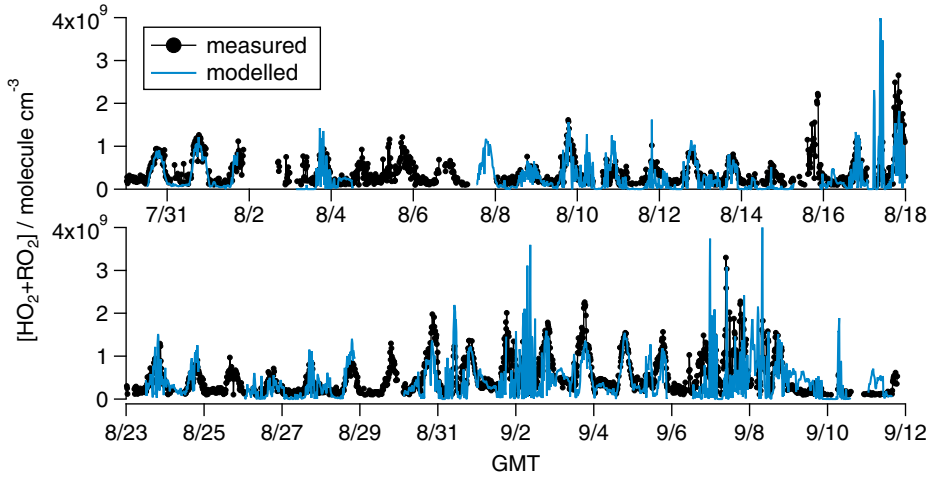


Fig. 2 Modelled and measured $\text{HO}_2 + \text{RO}_2$ during the TexAQS 2006 cruise of the R/V *Brown*

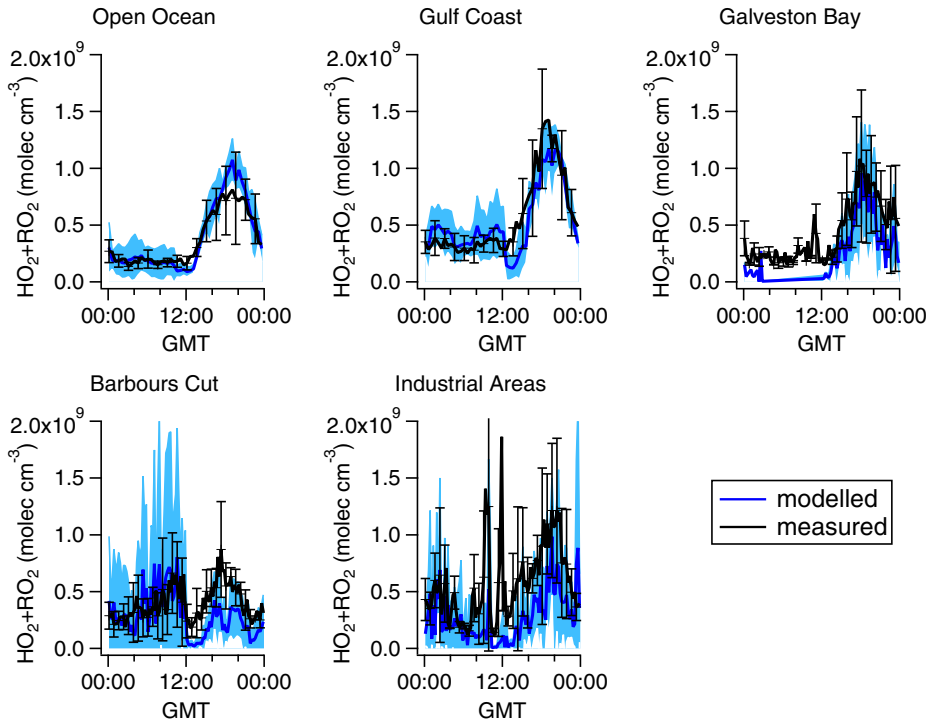


Fig. 3 Diurnal profiles of modelled and measured $\text{HO}_2 + \text{RO}_2$ in different regions during the TexAQS 2006 cruise of the R/V *Brown*. The lines are the averages; the shaded area and the bars are the $1\text{-}\sigma$ standard deviation of the model and of the measurements, respectively

profile of peroxy radicals, especially in the Open Ocean (e.g., July 30th and 31st as shown in Fig. 2), although there was large variability and scatter, as illustrated by the scatter plots in Figs. 4 and 5. This was in part due to actual variability in the model input data, especially in the most polluted areas, and in part related to the fact that the model constraints were measured at different frequencies (from 1 min to 30 min) thus forcing the model to interpolate the model constraints.

Day-time peroxy radicals The best agreement between the model and the measurements was in the Open Ocean and in the Gulf Coast during day-time (Fig. 3). In the Open Ocean, in the middle of the day, the model overestimated the measurements by <30%, on average. During the first four modelled days (July 30th to August 2nd, Fig. 2) the ship sampled air masses from the central Atlantic Ocean and the middle of the Caribbean Sea, which were the cleanest conditions encountered during the cruise and can be considered representative of background oceanic air. In the Gulf Coast, the model underestimated the measurements by 15–30%, in the middle of the day. In both areas the agreement was better in the early morning and in the late evening (within 20% or better). Conversely, in Galveston Bay and Barbours Cut, the model underestimated the measurements during the day by 30–40% and ~40%, on average (Fig. 3); in more polluted conditions, such as in the Industrial Areas, the model underestimated the measurements by up to 55%, although in this region it is

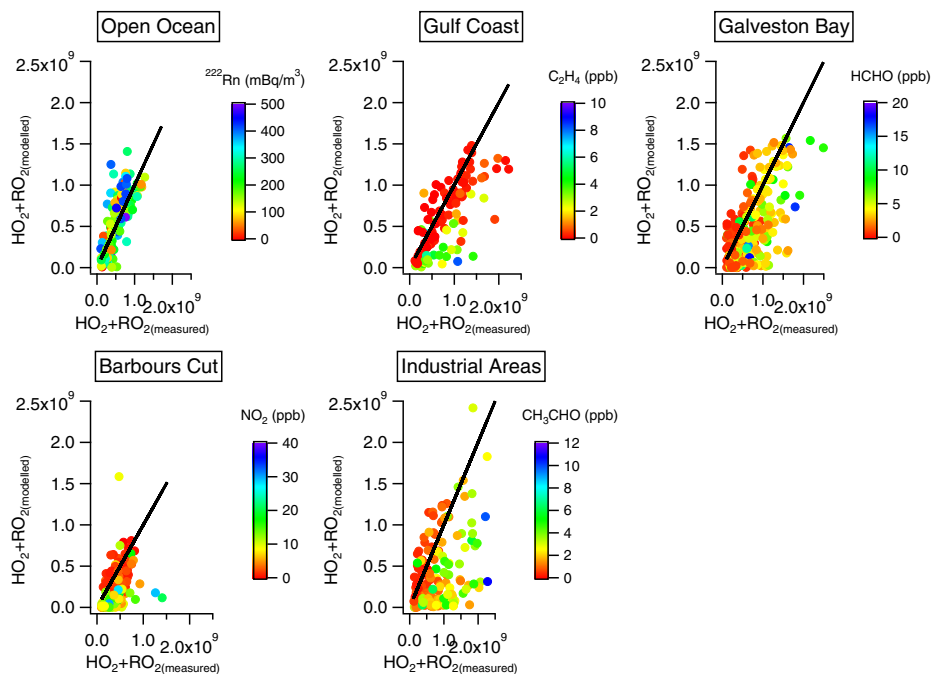


Fig. 4 Day-time modelled vs. measured $\text{HO}_2 + \text{RO}_2$ during the TexAQS 2006 cruise of the R/V *Brown*. The black line is the 1:1 line and the data are color-coded with different parameters in each region

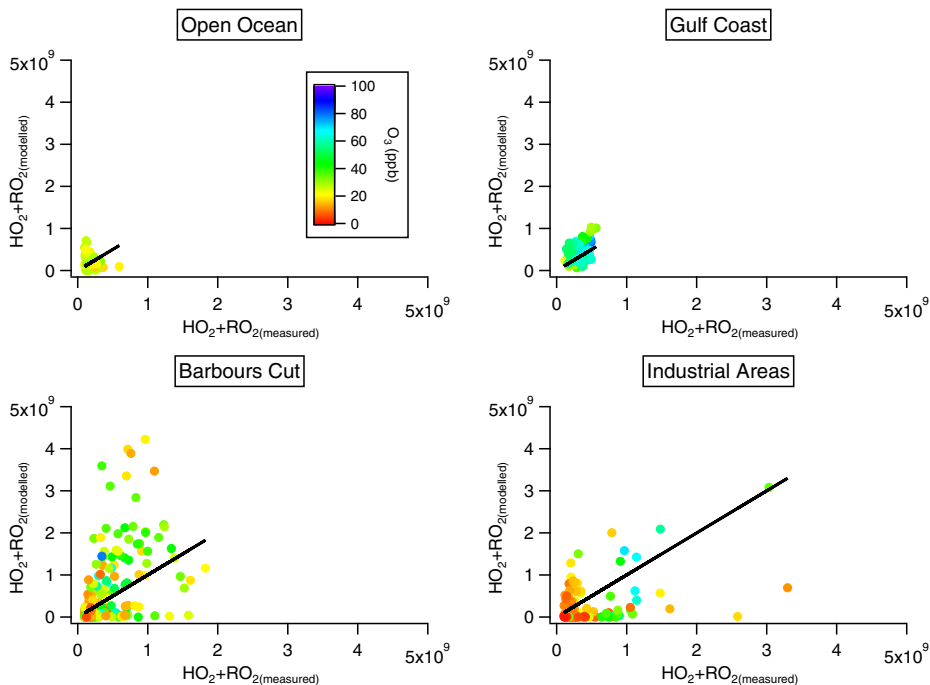


Fig. 5 Night-time modelled vs. measured $\text{HO}_2 + \text{RO}_2$ during the TexAQ5 2006 cruise of the R/V *Brown*. The black line is the 1:1 line and the data are color-coded with O_3 concentrations

more difficult to assess the level of agreement due to rapidly changing conditions and large variability.

Figure 4 shows scatter plots of day-time modelled vs. measured $\text{HO}_2 + \text{RO}_2$, color-coded with selected parameters to analyze the deviations from linearity. In the Open Ocean the model overestimated the measurements at higher ^{222}Rn counts, indicating that some air masses of continental origin were also sampled in this region; in the Gulf Coast, the model tended to underestimate the measurements at higher concentrations of alkenes and other pollution markers, such as NO_2 (Fig. 4). These events likely corresponded to specific emission sources, such as industries on the coast, other ships or oil extraction platforms in the Gulf. In Galveston Bay, Barbours Cut and in the Industrial Areas the model underestimated the measurements at higher concentrations of oxygenated VOCs, PANs, NO_2 (Fig. 4). The analysis of $\text{HO}_2 + \text{RO}_2$ and VOCs observations presented in Gilman et al. (2009), Sommariva et al. (2011) indicated that oxygenated VOCs in these areas were connected with aged air masses that were recirculated over Galveston Bay for several hours before coming back towards Houston.

In general, the model was more reliable under cleaner conditions in all regions. The dependence of the model-measurements disagreement on oxygenated VOCs and other secondary oxidation products in the polluted regions suggests that the discrepancy might be related to the description of carbonyl photochemistry in the MCM. One aspect of this problem is the formation of acyl peroxy radicals (e.g.,

CH_3CO_3 , $\text{C}_2\text{H}_5\text{CO}_3$, $\text{C}_3\text{H}_7\text{CO}_3$) from aldehydes and ketones, which will be discussed in more detail in Section 3.2.

Night-time peroxy radicals The R/V *Brown* did not spend much time in Galveston Bay at night, so this region will not be considered when discussing night-time chemistry. The agreement between modelled and measured $\text{HO}_2 + \text{RO}_2$ during night-time is more difficult to assess, owing to larger variability and scatter in both the model and the measurements (Figs. 2 and 5). In Barbour's Cut and in the Industrial Areas the agreement was typically within 40–50%, although sometimes it was within 20% (Fig. 3). In these areas the conditions often varied rapidly as plumes of NO_x and VOCs from industries and port operations affected the observations. However, as explained earlier, the model is not able to reproduce this high frequency variability because it does not have all the information that would be required; this was more of an issue at night, because during the day ozone (which was measured at high frequency) was a major driver for radical chemistry even under polluted conditions (Sommariva et al. 2011). On the other hand, the average night-time profiles (Fig. 3) showed reasonably good agreement (25–30%) under clean conditions (Open Ocean and Gulf Coast).

The analysis of the night-time scatter plots did not show any parameters clearly associated with the model-measurements disagreement. A weak correlation with NO_2 and O_3 was apparent in the Industrial Areas and, less clearly, in Barbour's Cut (Fig. 5): the model tended to overestimate the measurements at lower concentrations of O_3 and NO_2 and underestimate at higher concentrations of O_3 and NO_2 . Since ozonolysis reactions of VOCs were major sources of night-time peroxy radicals (Section 3.3), this might point to problems in the treatment of these reactions in the MCM, particularly with regard to their efficiency as radical sources. It is however difficult to identify any particular reaction or group of reactions, because the correlation was weak and no specific VOC was likewise correlated with the model-measurements disagreement.

Additional VOCs A key factor that determines the agreement between the model and the measurements is the degree to which all of the RO_2 precursors were included in the model. Some of the VOCs measured on the R/V *Brown* which are not included in the MCM occasionally accounted for a significant fraction of the OH reactivity during the R/V *Brown* cruise (e.g., vinyl acetate). There were likely also unmeasured VOCs, especially when the ship was in the more polluted Industrial Areas: the peroxy radicals formed by these VOCs were also not included in the MCM model results.

During the cruise, the GC-MS detected a peak corresponding to 2-methyl-2-butene and to acrolein. The two species could not be separated, therefore both VOCs were excluded from the model constraints. In order to evaluate the impact of additional VOCs on the concentration of RO_2 , a constraint was added to the model corresponding to a species with the same reactivity of 2-methyl-2-butene and the concentration determined by the co-eluted peak (average = 30 ppt; maximum = 670 ppt). The results showed that the modelled concentration of organic peroxy radicals increased by <5%, on average. However, RO_2 could increase by 20–25% (with a maximum of 35–40%) when large plumes of 2-methyl-2-butene + acrolein were sampled. The results show that modelled $\text{HO}_2 + \text{RO}_2$ was sensitive to concentrated plumes of reactive VOCs from specific sources, but less sensitive

to the background levels, even if they were influenced by mixing and dilution of similar plumes. These effects lead to the large variability observed in Figs. 2 and 3 for Barbours Cut and the Industrial Areas.

3.2 Peroxy radicals and PANs

It is difficult to assess the accuracy of the MCM model in calculating the concentrations of individual organic peroxy radicals, because there are no observations available. The only measurement available is the sum of peroxy radicals ($\text{HO}_2 + \text{RO}_2$) and it is possible that even if the modelled sum agreed reasonably well with the measured sum (Section 3.1), the individual species were not correctly represented. In fact, previous comparisons of peroxy radicals using MCM-based models have showed varying levels of agreement with the observations of HO_2 ; for example, the modelled concentration of HO_2 in the marine boundary layer often overestimated the observations (Carslaw et al. 1999, 2002; Sommariva et al. 2004, 2006) and sometimes underestimated them or showed good agreement (Carslaw et al. 1999; Emmerson et al. 2007; Whalley et al. 2010). This suggests that the MCM often underestimated and sometimes overestimated RO_2 . In addition, recent reports that some of the HO_2 measurements (by laser-induced fluorescence) suffer from interference under polluted conditions (Fuchs et al. 2011) indicate that the agreement between modelled and measured HO_2 might be worse, except on the occasions when the model underestimated HO_2 .

The analysis of the model results discussed in Section 3.1 indicated that, in the more polluted regions (Galveston Bay, Barbours Cut, Industrial Areas), at high concentrations of oxygenated VOCs, the model underestimated the $\text{HO}_2 + \text{RO}_2$ measurements; this might indicate that the model underestimated the concentrations of acyl peroxy radicals formed by the oxidation of oxygenated VOCs. Each acyl peroxy radical is the precursor of a single PAN species (e.g., CH_3CO_3 for PAN and $\text{C}_2\text{H}_5\text{CO}_3$ for PPN). The model can be used to calculate a realistic concentration of PAN species under certain conditions: if transport is not a dominant factor in determining the concentrations of PANs and if their background concentrations can be neglected. At the average (15:00–21:00 GMT, 10:00–16:00 Local Time) conditions in Barbours Cut during the R/V *Brown* cruise ($\text{NO} = 9.3 \times 10^{10}$ molecule cm^{-3} , $\text{NO}_2 = 1.5 \times 10^{11}$ molecule cm^{-3} , Temperature = 303 K) the net lifetime of PAN—i.e., the lifetime calculated accounting for the reformation of PAN in the presence of NO_2 —is ~ 45 min, comparable to the interval between two consecutive inputs of VOCs in the model (determined by the sampling frequency of the GC instrument). The observations reported by Roberts et al. (2003) at LaPorte, Texas, approximately 10 km West of Barbours Cut (Fig. 1), clearly showed that PAN was photochemically formed in this area, with concentrations decreasing to below the instrument's detection limit during the night (evidence of very low background values). Under these conditions, the agreement between modelled and measured PANs can be used as diagnostic tools to qualitatively assess how well the MCM model calculates the concentration of some individual RO_2 .

Modelled and measured PAN and PPN average profiles during day-time in Barbours Cut are shown in Fig. 6. The model underestimated PAN in the morning by 30–40%, but overestimated it by 25% in the afternoon (after 19:00 GMT, 14:00 Local Time). On the other hand, the model agreed reasonably well with measurements of

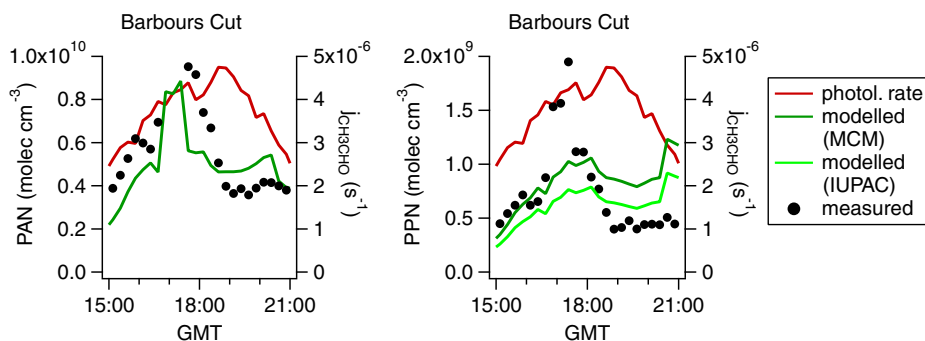


Fig. 6 Average day-time profiles of modelled and measured PAN, PPN in Barbours Cut during the TexAQS 2006 cruise of the R/V *Brown*

PPN in the morning (within 20%), but overestimated measured PPN by approximately a factor of 2 in the afternoon (Fig. 6). The uncertainty in the observations was 15% (Section 2.1). This analysis requires that the source and the sink terms of PANs are well constrained in the model. The MCM v3.1 uses the same kinetic parameters for both PAN and PPN (Jenkin et al. 1997; Saunders et al. 2003). While the PAN kinetic data are consistent with the IUPAC recommendations (Atkinson et al. 2006), the PPN rate coefficients are different. The rate coefficient for the formation reaction is 11% lower and the rate coefficient for the decomposition reaction is 20% higher than those used in the MCM v3.1 (Seefeld and Kerr 1997; Kirchner et al. 1999; Atkinson et al. 2006): using the recommended rate coefficients instead of the MCM rate coefficients resulted in lower ($\sim 26\%$) modelled concentrations of PPN (Fig. 6), slightly improving the agreement with the measurements in the afternoon. Given the limitations of the modelling approach, the agreement between the model and the measurements can be considered satisfactory for PAN, but less so for PPN, suggesting that the MCM underestimates the concentration of $C_2H_5CO_3$ (and possibly of other acyl peroxy radicals) by as much as a factor of two, especially in the morning and in the central part of the day (i.e., before 14:00).

3.3 Composition of the peroxy radicals pool

The explicit treatment of chemistry in the MCM allows the calculation of the concentrations of individual organic peroxy radicals (RO_2), which could not be measured during TexAQS 2006. The relative importance of each peroxy radical in an air mass depends on the VOC composition of the air mass. Figure 7 shows the average modelled fraction of total peroxy radicals constituted by HO_2 , CH_3O_2 , $CH_3SCH_2O_2$ and selected organic peroxy radicals in the five regions of the R/V *Brown* cruise (Fig. 1). In the following discussion, only the most abundant peroxy radicals have been considered: the sum of the selected peroxy radicals accounted for at least 85% of modelled $HO_2 + RO_2$ during day-time. The remaining fraction of modelled $HO_2 + RO_2$ consisted of a large number of organic peroxy radicals, mostly derived by long-chain VOCs and secondary oxidation products, each accounting for a small percentage of the total; this fraction was proportionally smaller in the more polluted

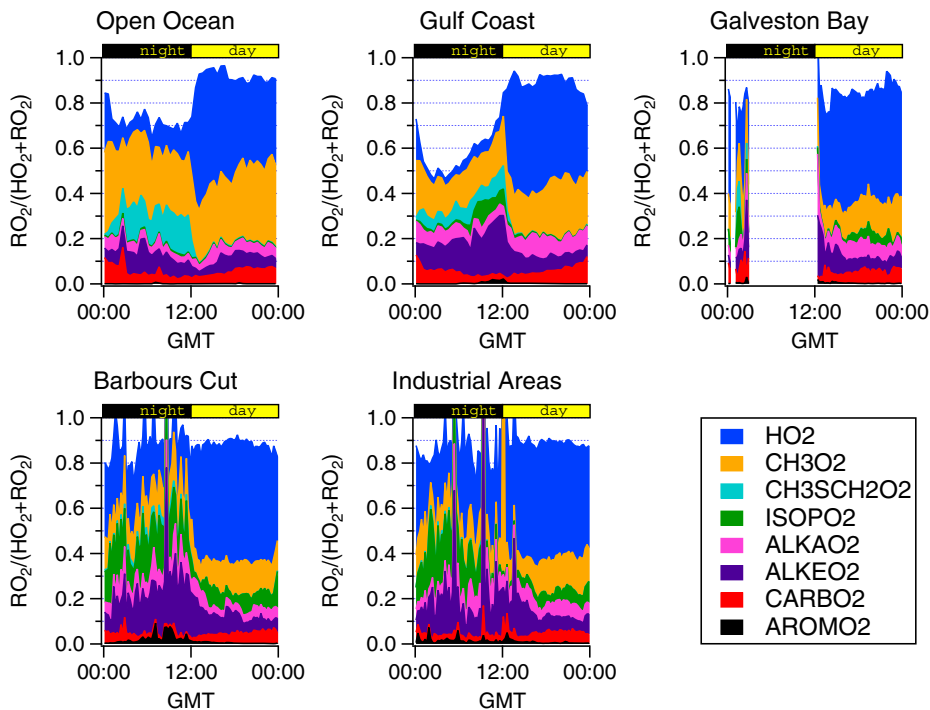


Fig. 7 Average modelled $\text{RO}_2/(\text{HO}_2 + \text{RO}_2)$ ratios in different regions during the TexAQ5 2006 cruise of the R/V *Brown*. See [Appendix](#) for the RO_2 codenames

regions (Fig. 7), where continuous emissions of primary VOCs of industrial origin controlled the concentrations of the peroxy radicals precursors.

The selected organic peroxy radicals were divided into five classes (ISOPO₂, ALKAO₂, ALKEO₂, CARBO₂, AROMO₂), roughly corresponding to the functionality of their main VOC precursors (biogenics, alkanes, alkenes, carbonyls, aromatics). The classification is not straightforward because most peroxy radicals have more than one VOC precursor and often these have different functional groups: additionally, small RO₂ are often formed from the fragmentation of longer carbon chains (Sommariva et al. 2008, 2011). The peroxy radicals included in the five classes (ISOPO₂, ALKAO₂, ALKEO₂, CARBO₂, AROMO₂) and the lists of their corresponding precursors are given in [Appendix](#).

During the day, HO₂ was always the dominant peroxy radical, accounting for ~50% of the total in all regions; the single most important organic peroxy radical during the day was always CH₃O₂, which accounted for ~30% of the total in the Open Ocean, 20–25% in the Gulf Coast and ~15% in the more polluted areas around Houston, Texas (Fig. 7). Day-time radical chemistry under clean conditions is dominated by the reactivity of CO and CH₄, the main precursors of HO₂ and CH₃O₂, which explains why in the Open Ocean they accounted together for ~80% of HO₂ + RO₂. Oxygenated VOCs (HCHO) and light alkenes (ethene, propene), which were the most important OH sinks in the Open Ocean besides CO and CH₄ (Gilman et al. 2009), are also efficient sources of HO₂ and CH₃O₂; moreover, the

third and the fourth most important contributions ($\sim 8\%$ and $\sim 7\%$, respectively) to the RO_2 pool were from the other organic RO_2 formed from oxygenates and light alkenes (CARBO2 and ALKEO2, [Appendix](#), Fig. 7).

By contrast, under more polluted conditions (Galveston Bay, Barbours Cut and Industrial Areas) the contribution of methyl peroxy radical to the RO_2 pool decreased, while the contributions from VOCs (mostly alkenes and oxygenates) increased up to 35% of total $\text{HO}_2 + \text{RO}_2$ (Fig. 7). Gilman et al. (2009) estimated that most of the reactivity of OH in the Industrial Areas was due to the oxidation of alkenes and other highly reactive species (e.g., di-alkenes) and of light (C2-C4) alkanes (corresponding to ALKAO2 and ALKEO2 peroxy radicals, respectively, in Fig. 7). The contribution from aromatics was almost always negligible, except for occasional plumes, but there were significant contributions (7–9%) from isoprene-related peroxy radicals in Barbours Cut and in the Industrial Areas. Isoprene and other biogenic VOC were also present at night and contributed significantly to the RO_2 pool (20–30%) and to the reactivity of the nitrate radical (Section 4.2) in these regions. Gilman et al. (2009) concluded, on the basis of the observed diurnal profile, that isoprene in the Houston area was mostly biogenic in origin and partly from industrial sources, but there is evidence (Kuster et al. 2004; Stutz et al. 2010) that night-time isoprene concentrations were largely related to industrial emissions.

At night HO_2 accounted for only 10% in the Open Ocean, but up to 20–30% in the Industrial Areas (Fig. 7). On the other hand the fraction of $\text{HO}_2 + \text{RO}_2$ constituted by CH_3O_2 remained approximately the same as during the day in all regions (Fig. 7). In general, in the Industrial Areas there was less variability between day and night, as far as the composition of the RO_2 pool is concerned, because industrial emissions of VOCs were continuous and did not follow a diurnal cycle. In the Open Ocean and, to a lesser extent, in the Gulf Coast, $\text{CH}_3\text{SCH}_2\text{O}_2$ —the peroxy radical formed by the reaction of DMS with NO_3 —contributed to a significant fraction to $\text{HO}_2 + \text{RO}_2$: 15–20% and $\sim 10\%$, respectively. However, DMS oxidation did not contribute significantly to day-time peroxy radicals, in accord with the findings of Gilman et al. (2009) that DMS was not an important reactant for OH during the R/V *Brown* cruise.

A discussion about the formation of peroxy radicals and, hence, ozone from different classes of VOCs in the Houston area has been presented in Sommariva et al. (2011). In that paper it was shown how photochemical formation of ozone was linked to different classes of VOCs, depending on the sources in each region. Combining that analysis and the speciation of peroxy radicals obtained with the MCM, the individual VOCs and peroxy radicals that most contributed to photochemical ozone formation can be identified. For example, in Barbours Cut, Sommariva et al. (2011) found that the highest ozone formation rates were related to E-SE air masses rich in oxygenated and biogenic VOCs, followed by E-NE and W-SW air masses rich in alkenes: this is consistent with the analysis shown in Fig. 7, which shows that, besides HO_2 and CH_3O_2 , the most important contributors to the RO_2 pool were the ISOPO2 and CARBO2 peroxy radicals, which were mostly derived from the oxidation of isoprene, carbonyls and long-chain alkenes ([Appendix](#)).

3.4 Case study: Jacinto Point

The complexity of the RO_2 pool composition is well illustrated by the events during the night of September 7th, when the R/V *Brown* was in Jacinto Point, on the North

side of the Houston Ship Channel entrance (Fig. 1). The maximum $\text{HO}_2 + \text{RO}_2$ concentrations observed during TexAQS 2006 were measured during this night: 134 ppt and 123 ppt ($= 3.35 \times 10^9$ and 3.1×10^9 molecule cm^{-3}) around 9:30 GMT (4:30 Local Time) and a second peak of 82 ppt (2.05×10^9 molecule cm^{-3}) about two hours later. These peaks were clearly correlated with changes in the local wind direction (Fig. 8), indicating that plumes emitted from nearby industries were being sampled.

The composition of these plumes was a complex mixture of VOCs, including alkanes (up to 450 ppb of n-butane) and a range of light alkenes, some of which are

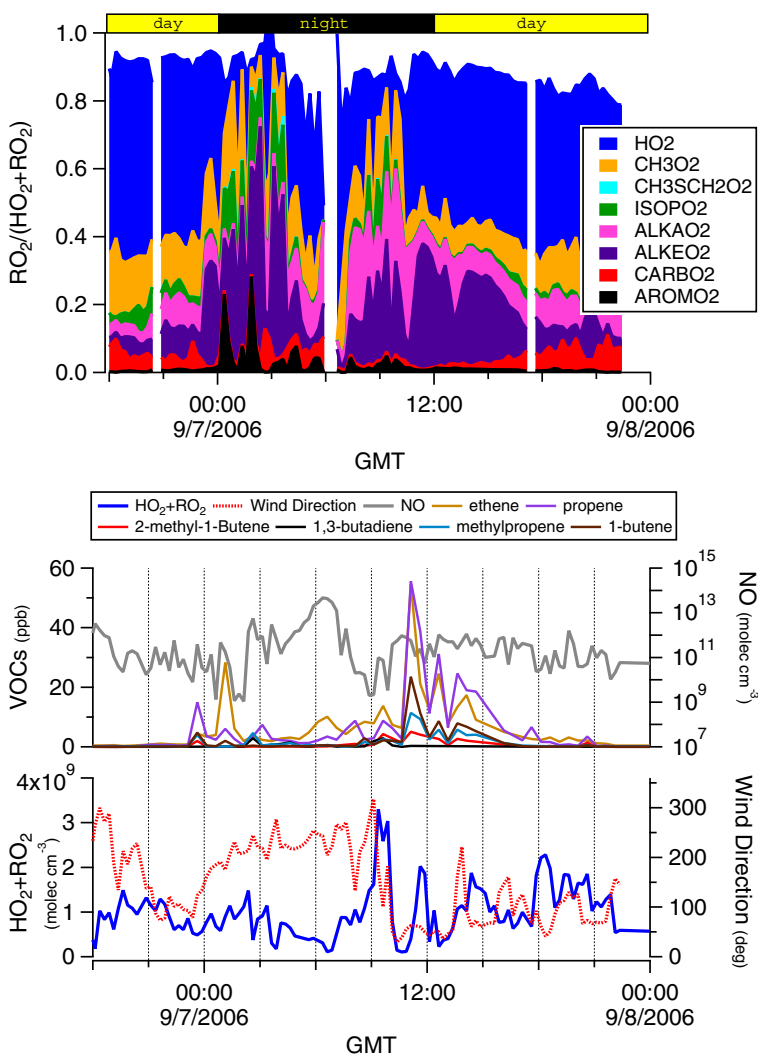


Fig. 8 Modelled $\text{RO}_2/(\text{HO}_2 + \text{RO}_2)$ ratios (*top*) and measured concentrations of selected species (*bottom*) during the night of September 7th at Jacinto Point, near the entrance of the Houston Ship Channel (HSC in Fig. 1). See [Appendix](#) for the RO_2 codenames

shown in Fig. 8. The concentration of NO between 9:00–12:00 GMT (4:00–7:00 Local Time) ranged between 800 ppt (2.0×10^{10} molecule cm^{-3}) and 38 ppb (9.5×10^{11} molecule cm^{-3}), which excludes any significant contribution to VOCs oxidation by the nitrate radical, since NO_3 is efficiently destroyed by reaction with NO. This means that the formation of the peroxy radicals observed in Jacinto Point was related to ozonolysis reactions (Fig. 9) and therefore to the alkenes in the sampled plumes. The most abundant alkenes in the two plumes were ethene and propene (14 ppb and 9 ppb, respectively, in the 9:30 plume, and up to 55 ppb each in the 11:30 plume); based on the local wind direction, the earlier plume came from the South and the later plume came from East-Northeast indicating that they were from two different industrial sources (Fig. 8). The composition was also different: the 9:30 plume contained lower concentrations of ethene and propene and up to 3 ppb of 1,3-butadiene, while the 11:30 plume contained higher concentrations of 1-butene and methylpropene (up to 23.5 ppb and 11.3 ppb, respectively) and less than 300 ppt of 1,3-butadiene.

The composition of the peroxy radicals pool (Fig. 8) clearly changed throughout the night of September 7th, as different air masses were being sampled. For example, HO_2 accounted for about 12% of $\text{HO}_2 + \text{RO}_2$ at 9:00 GMT, but 4–5% during the 9:30 plume and $\sim 47\%$ during the 11:30 plume. The MCM analysis also showed that the first plume was composed almost equally of ALKAO2 and ALKEO2 peroxy radicals (20–30%), while the second plume was richer in ALKEO2 peroxy radicals ($\sim 37\%$). The difference between the two plumes can be explained from the breakdown of the individual radical species: with the exception of 1-butadiene, the concentrations of most alkenes, and especially of ethene and propene, were much higher in the

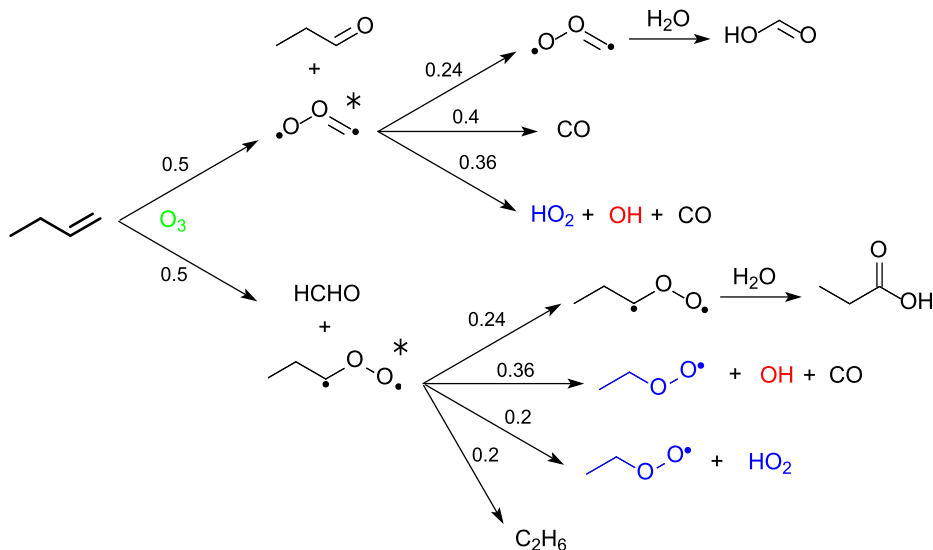


Fig. 9 Formation of radicals from the ozonolysis of alkenes (1-butene in this example) in the MCM v3.1 (Saunders et al. 2003). Peroxy radicals are highlighted in blue, OH in red; the numbers are the branching ratios

11:30 plume than in the 9:30 plume. Since ozonolysis of alkenes promptly forms HO₂ (Fig. 9), this explains why HO₂ was a much larger contributor to the HO₂ + RO₂ pool in the 11:30 plume. However, in the presence of such high concentrations of NO (Fig. 8), HO₂ reacted to form OH, which could readily react with the alkenes to form OH-added peroxy radicals (e.g., HOCH₂CH₂O₂, HYPROPO₂, IPROPOLO₂, etc...). The peroxy radicals formed by addition of OH reactions are included in ALKEO₂ (Appendix), while the peroxy radicals formed by ozonolysis reactions (e.g., C₂H₅O₂, NC₃H₇O₂, IC₃H₇O₂, etc...) are included in ALKAO₂ (Appendix), which explains why ALKEO₂ was proportionally a larger contributor to HO₂ + RO₂ in the second plume than in the first plume. Night-time formation of OH (Fig. 9) was occurring in both plumes, but the concentration of OH was very different: the MCM model calculated $<1 \times 10^5$ molecule cm⁻³ during the first event and $>3 \times 10^6$ molecule cm⁻³ during the second event, so the formation of RO₂ by addition of OH to alkenes (ALKEO₂) was a much larger factor in the latter.

4 Nitrate radical (NO₃)

4.1 Model-measurements comparison for nitrate radical

The MCM model was used to calculate the concentrations of NO₃ and N₂O₅ during the R/V *Brown* cruise. The NO₃–N₂O₅ chemical system is schematically represented in Eqs. 2–5, where X is a generic sink for NO₃ (e.g., reactions with NO, VOCs and photolysis) and Y is a generic sink for N₂O₅ (e.g., aerosol uptake, hydrolysis):



The model is designed for fast reacting species, such as OH and peroxy radicals, and it does not include vertical or horizontal transport. As such, the model results can be considered reliable only under conditions where the reactivity of NO₃ is rapid, but are less reliable where reactivity is slow. A model calculation based on integration from one observed data point to the next in a time series may generate error if the lifetime of the calculated species (NO₃ in this case) is long with respect to the model time steps. In this case, changes due to air mass shifts (i.e., transport) will not be properly represented. Such errors should lead to over and under-predictions with equal probability if there are random changes in the air mass between successive measurements due to transport or to the movement of the ship. NO₃ levels controlled by industrial emissions of highly reactive VOCs or by marine emissions of DMS can be considered suitable for modelling with a zero-dimensional box-model.

The concentrations of NO₃ (and N₂O₅) were calculated for 20 nights of the R/V *Brown* cruise, mostly during the second half of each leg when the ship spent more time in semi-polluted and polluted areas than in the clean marine boundary layer. The full comparison between the model results and the measurements is shown

in Fig. 10 as a time series and the average night-time profiles of NO_3 for each region are shown in Fig. 11. The measured concentrations were often below the detection limit ($5.0 \times 10^7 \text{ molecule cm}^{-3}$) of the CaRDS instrument under very clean and very polluted conditions. For example, on the nights of August 13th, 14th and 15th, the R/V *Brown* was in Barbour's Cut and sampled air masses influenced by local sources with concentrations of NO of about 10 ppt, with peaks of ppb level: on those nights NO_3 was below the instrumental detection limit, due to the fast reaction with NO, which was well reproduced by the model (Fig. 10).

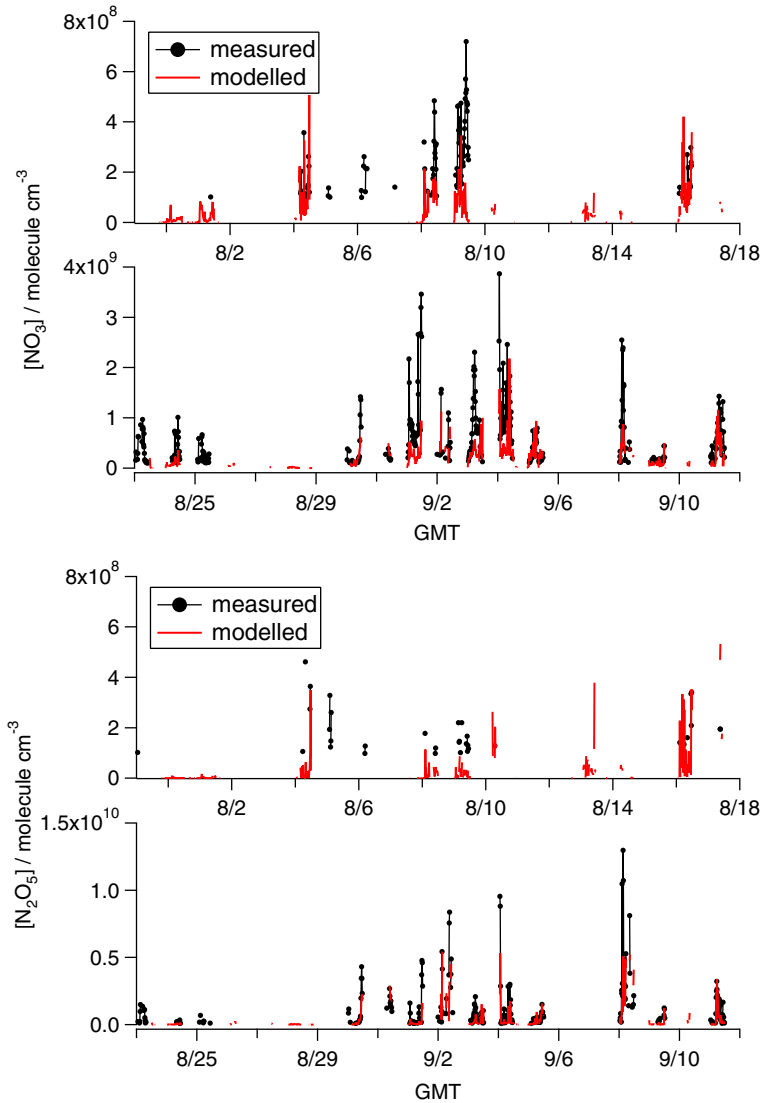


Fig. 10 Modelled and measured NO_3 , N_2O_5 during the TexAQS 2006 cruise of the R/V *Brown*. For clarity, the two parts of the cruise are plotted on different scales

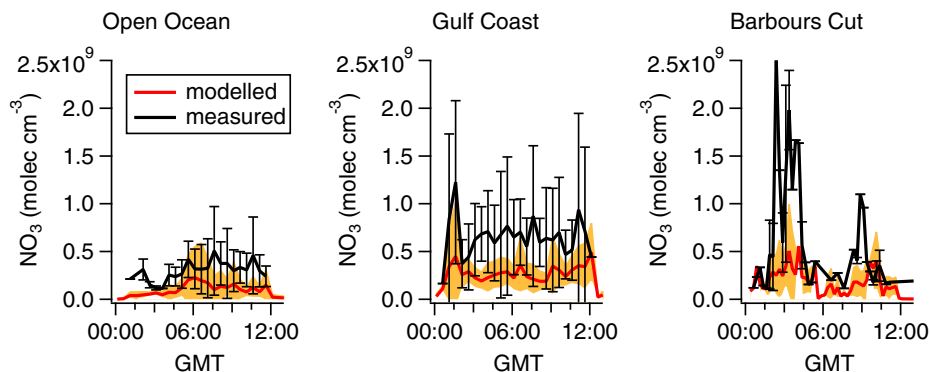


Fig. 11 Night-time profiles of modelled and measured NO_3 in different regions during the TexAQS 2006 cruise of the R/V *Brown*. The lines are the averages; the shaded area and the bars are the 1- σ standard deviation of the model and of the measurements, respectively

In general, the model underestimated the observations during the entire R/V *Brown* cruise. The average modelled-to-measured ratios were different in each region (Fig. 11): ~ 0.3 in the Open Ocean, ~ 0.4 in the Gulf Coast and in Barbour's Cut. Data in Galveston Bay and Industrial Areas were too sparse to provide a meaningful statistics. The agreement between the model and the measurements was similar for N_2O_5 , with a campaign average modelled-to-measured ratio of ~ 0.4 . These results are in contrast with a previous study which used a similar modelling approach (Sommariva et al. 2009): during the NEAQS 2004 cruise, the model overestimated the measurements by 30–50%, on average. During NEAQS 2004, the concentrations of NO_3 were typically a factor of 6–8 smaller and the NO_3 production rates ($k_2 \times [\text{O}_3] \times [\text{NO}_2] + k_{-3} \times [\text{N}_2\text{O}_5]$) were typically a factor of 10–12 smaller than during TexAQS 2006. The comparison of the two studies suggests that under conditions of larger NO_3 production rate the model tends to underestimate NO_3 : the reason for this difference is otherwise difficult to assess.

Additional VOCs In order to evaluate the impact of additional VOCs on the concentration of NO_3 – N_2O_5 system (Eq. 4), a constraint was added to the model, corresponding to a species with the same reactivity of 2-methyl-2-butene and the concentration determined by the co-eluted chromatographic peak 2-methyl-2-butene + acrolein (Section 3.1). The model results showed a decrease in the modelled concentrations of NO_3 (and N_2O_5) of $\sim 10\%$, on average, and up to 40% during the largest plume of 2-methyl-2-butene event. The addition of a highly reactive species could therefore improve agreement on the occasions when the model overestimated the measurements (Fig. 10). The concentration attributed to 2-methyl-2-butene was about 20 ppt on that night, but it suggests that other unmeasured VOCs might have been present. It must be noted, however, that emissions of VOCs were often coincidental with emissions of NO in the proximity of industrial activities and/or ship plumes. Since even low concentrations of NO would deplete the concentration of NO_3 , the presence of unmeasured/unknown VOCs could explain the model-measurement discrepancies only under low NO concentrations.

N_2O_5 uptake One of the key parameters that control the concentration of NO_3 is the uptake coefficient of N_2O_5 ($\gamma_{N_2O_5}$, Eq. 5) on aerosol. Several studies have demonstrated the variability of $\gamma_{N_2O_5}$ in the lower atmosphere, due to the variability in the composition of aerosol, ambient relative humidity and temperature. In this work, the base model used a constant $\gamma_{N_2O_5} = 0.02$ (Section 2.1, Aldener et al. 2006). In order to test the sensitivity of the calculated concentrations of NO_3 to aerosol uptake under the conditions of TexAQS 2006, the model was run with $\gamma_{N_2O_5} = 0.001$ (Brown et al. 2006) and with $\gamma_{N_2O_5} = 0$. The results showed that the concentration of NO_3 increased, on average, by about 17% and 18%, respectively, due to slower or lack of removal of N_2O_5 via aerosol uptake (Fig. 12). Since the uptake rate is linearly dependent on the aerosol surface area (A , Eq. 1), the model showed a similar sensitivity to the aerosol surface area: varying A by a factor of 2 resulted in a change of about $\pm 9\%$ in the modelled concentration of NO_3 .

A slower uptake rate for N_2O_5 (because of lower $\gamma_{N_2O_5}$ and/or aerosol surface area) would improve the agreement between the model and the measurements. Suppression of $\gamma_{N_2O_5}$ has been correlated to organic-rich particles (Brown et al. 2006); however, submicron particles measured during TexAQS 2006 when the R/V *Brown* was near the polluted areas or during periods of continental outflow were largely inorganic (only 22–36% of organic matter, Bates et al. 2008). It must also be noted that a $\gamma_{N_2O_5}$ value of the order of 0.001 is inconsistent with $ClNO_2$ production from heterogeneous uptake of N_2O_5 , which was observed during the R/V *Brown* cruise (Osthoff et al. 2008).

These results suggest that additional loss terms for N_2O_5 , e.g., the gas-phase hydrolysis which has been suggested as potential sink by laboratory experiments (Mentel et al. 1996; Wahner et al. 1998) would result in a larger discrepancy between the model and the measurements. This is in accord with some of the previous studies of the nitrate radical chemistry (Aldener et al. 2006; Brown et al. 2006), although it is in contrast with others (Ambrose et al. 2007; Sommariva et al. 2009). The model response to changes in the uptake coefficient of N_2O_5 indicate relatively low sensitivity to N_2O_5 sinks, suggesting that the concentrations of the nitrate radical during TexAQS 2006 were controlled by NO_3 sinks instead.

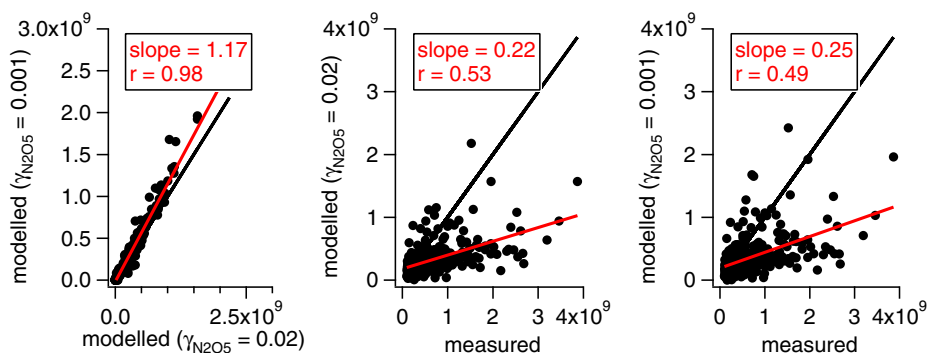


Fig. 12 *Left:* comparison of modelled NO_3 calculated with $\gamma_{N_2O_5} = 0.02$ and with $\gamma_{N_2O_5} = 0.001$. *Middle:* modelled vs measured NO_3 with $\gamma_{N_2O_5} = 0.02$. *Right:* modelled vs measured NO_3 with $\gamma_{N_2O_5} = 0.001$. The black lines are the 1:1 lines and the red lines are the linear fits

4.2 Nitrate radical budget and interactions with RO₂

The nitrate radical has only one well known source, the reaction between NO₂ and O₃ (Eq. 2). The sinks, however, are more uncertain: besides the equilibrium reaction with NO₂ to form N₂O₅, NO₃ reacts with a large number of VOCs, with peroxy radicals and, if present, with NO. The relative importance of each sink term determines the impact of NO₃ chemistry on the composition of the troposphere. For example, reactions with some VOCs form organic nitrates, which act as reservoirs of nitrogen and have been linked to the formation of secondary organic aerosol (Brown et al. 2009); the reaction with DMS can be the most important process controlling the oxidation of this species (Osthoff et al. 2009) and the reactions with peroxy radicals can generate night-time OH radicals (Vaughan et al. 2006). The measurements of NO₃, VOCs and HO₂ + RO₂ made during TexAQS 2006 were used to calculate the first-order loss rate of NO₃ during the R/V *Brown* cruise. The results—averaged and divided according to the location of the ship—are shown in Fig. 13a, b. Data from Galveston Bay were neglected in the following analysis because too few data were taken in this region during the night.

Alkanes and aromatics were negligible contributors to the gas-phase removal of NO₃ and oxygenated VOCs contributed up to 2% only in the Gulf Coast. The major sinks for NO₃ in all regions were alkenes, biogenic VOCs, DMS and peroxy radicals (Fig. 13b). In the Open Ocean and in the Gulf Coast, the most important NO₃ sink was DMS (79% and 38%, respectively). This is consistent with the modelled composition of the peroxy radicals pool during the night discussed earlier (Fig. 7, Section 3.3), which showed a significant presence of CH₃SCH₂O₂. DMS was a significant sink also in the more polluted areas, although it was much less important than alkenes (19–26%) and biogenic VOCs (50–58%). As explained above (Section 3.3), biogenic VOCs also have industrial origin and this was likely the case in Barbours Cut and the Industrial Areas at night-time (Stutz et al. 2010), since emissions from vegetation typically follow a diurnal cycle.

Peroxy radicals were important contributors to the gas-phase removal of NO₃, especially in the less polluted areas. In the more polluted areas (Barbours Cut and Industrial Areas) the contribution of peroxy radicals was comparable to those of aromatics and more important than alkanes and oxygenated VOCs (1–2%). Since HO₂ was typically a minor component of the peroxy radicals pool during the night (Fig. 7) this loss process can mostly be attributed to the reaction of NO₃ with organic peroxy radicals. In the Open Ocean, peroxy radicals were the second most important NO₃ sink after DMS (12%) and in the Gulf Coast they were the third most important NO₃ sink after DMS and alkenes (28%).

The numbers shown in Fig. 13b can be compared with those reported by Brown et al. (2011), derived by three flights around Houston, Texas, in October 2006. In air masses advected from the Houston Ship Channel, biogenic and oxygenated VOCs contributed ~15% and ~18%, respectively, to the gas-phase loss of NO₃. This is very different from the budget calculated from the ship data when the R/V *Brown* was in Barbours Cut or in the Industrial Areas (Fig. 13b) which show much smaller contribution from oxygenated VOCs (~1%) and much higher contribution from biogenic VOC (50–58%). The R/V *Brown* data were closer to the source than the aircraft data, so much of the biogenics were oxidized during transport and secondary products (such as oxygenates) were more important a few miles downwind of the

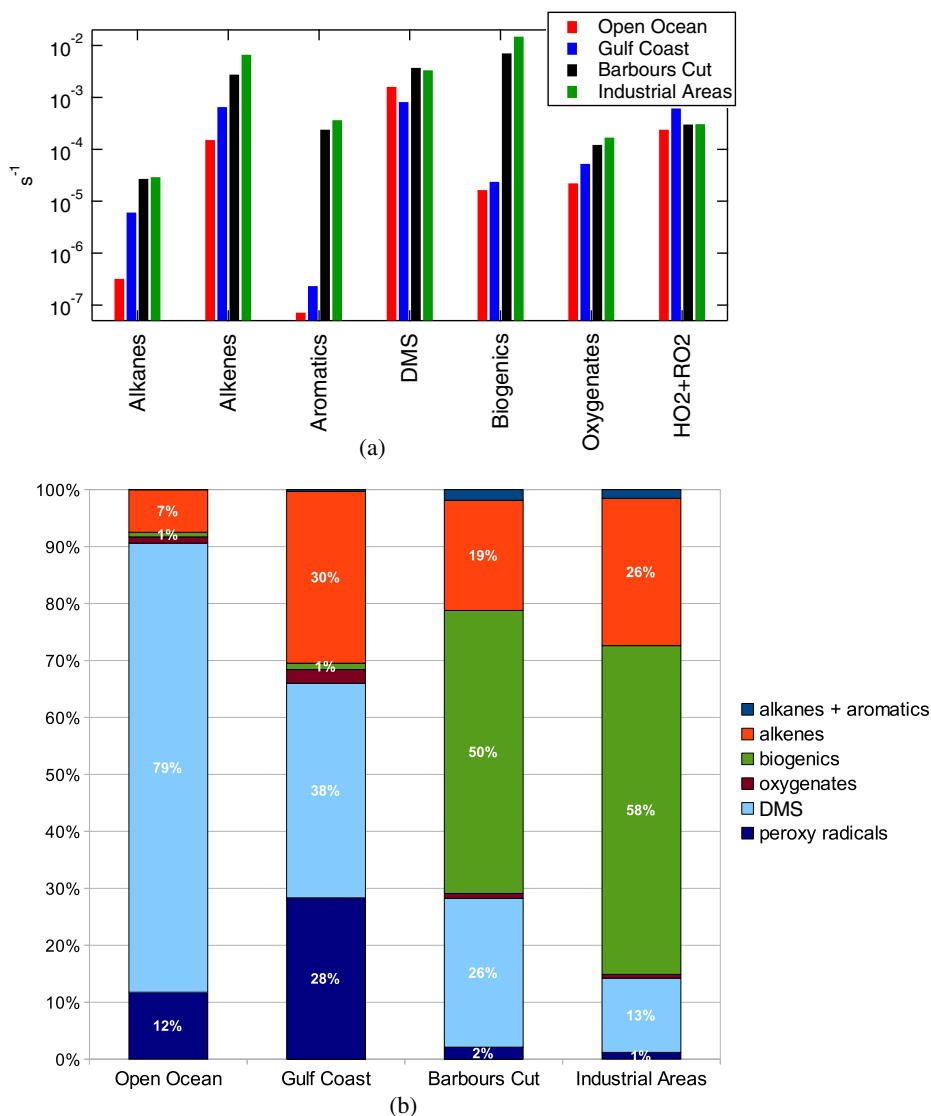
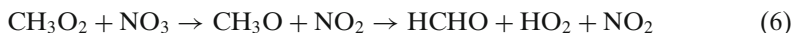


Fig. 13 Average measured first-order loss terms for NO_3 between 01:00 and 11:00 GMT (20:00–06:00 local time) in different regions during the TexAQs 2006 cruise of the R/V *Brown*: **a** absolute values in s^{-1} , **b** relative values in %

emission sources. Brown et al. (2011) calculated that peroxy radicals contributed 4–5% to the total loss of NO_3 ; this is larger than 1–2% observed in Barbours Cut and in the Industrial Areas (Fig. 13b), which are near the emission sources and where primary VOCs concentrations were high. However, it is much smaller than 12–28% observed on the R/V *Brown* in the Open Ocean and in the Gulf Coast (Fig. 13b): both of these are downwind regions, as were those sampled by the aircraft in Brown et al. (2011), but peroxy radicals were measured on the R/V *Brown* while they were estimated on the aircraft (based on PANs observations).

The importance of $\text{RO}_2 + \text{NO}_3$ reactions as sinks for the nitrate radical has been noted previously: for example, the model study by Sommariva et al. (2009) determined that RO_2 accounted on average for $\sim 20\%$ of the NO_3 losses in a semi-polluted environment; the observations reported here clearly support this view and the model results were consistent with the previous study. The implications of organic peroxy radicals being a major sink for NO_3 are yet unclear, mostly because the kinetic database of this type of reaction is limited (Canosa-Mas et al. 1996; Vaughan et al. 2006). These reactions are known to form NO_2 and HO_2 , which can be a source of ozone at sunrise and a source of OH at night, respectively. For example, in the case of methyl peroxy radical:



The formation of OH via these night-time reactions occurs largely via the reaction of HO_2 with O_3 , as NO concentration must be very low (otherwise it would titrate NO_3). In turn, the oxidation of VOCs will form other RO_2 , starting a positive feedback on the concentrations of radical species that can significantly enhance the oxidation of VOCs at night, as long as NO_3 production is sustained. On the other hand, the sequence of reactions in Eq. 6 decreases the night-time removal of NO_x (via $\text{NO}_3 + \text{NO}_2 \rightleftharpoons \text{N}_2\text{O}_5 \xrightarrow{\text{aerosol}} \text{HNO}_3$ and $\text{NO}_3 + \text{VOCs} \rightarrow \text{HNO}_3$ reactions, followed by HNO_3 deposition) resulting in more NO_2 being available at sunrise to form ozone. It is, however, not possible to quantify this effect with a box-model in which both NO_2 and O_3 were constrained to the observations (Section 2.1).

5 Summary

During the TexAQs 2006 cruise of the R/V *Brown* observations of total peroxy radicals ($\text{HO}_2 + \text{RO}_2$) and nitrate radical (NO_3) were taken in the Atlantic Ocean, in the Gulf of Mexico and in the industrial regions around Houston, Texas. These measurements were compared with the results of a box-model based upon the Master Chemical Mechanism (MCM) and constrained to the chemical and physical parameters measured onboard the R/V *Brown*. The model could reproduce the observations of $\text{HO}_2 + \text{RO}_2$ during the day to within $\sim 40\%$, on average. In the unpolluted regions, the agreement was better, both during day-time (15–30%) and during night-time (25–30%). The analysis of the model results suggests that the model underestimated the measurements particularly in aged air masses, e.g., at high levels of oxygenated VOCs, and that the MCM might underestimate the concentrations of some acyl peroxy radicals and, possibly, of other short-chain RO_2 .

The information included in the MCM was used to estimate the relative importance of individual peroxy radicals in various regions of the R/V *Brown* cruise and, in particular, at Jacinto Point, a location near the Houston Ship Channel where the highest concentrations of $\text{HO}_2 + \text{RO}_2$ were observed (134 ppt) during the night. The break-down of the RO_2 pool indicated that HO_2 constituted $\sim 50\%$ of the peroxy radical pool during the day and between 10% and 30% during the night. During the night, isoprene—which was in part of industrial origin—contributed up to 30% to the RO_2 pool in the Industrial Areas, and DMS $< 20\%$ in the unpolluted regions.

The model consistently underestimated the measurements of NO_3 , especially in the Open Ocean: the typical model-to-measurements ratio was 0.3–0.4. The

agreement between the model and the measurements could be slightly improved by using a lower uptake coefficient for N_2O_5 on sub-micron aerosol, although this cannot be justified during TexAQS 2006 where submicron aerosol was mostly inorganic. The nitrate radical budget—calculated from the measurements—indicated that DMS, alkenes and RO_2 were the most important NO_3 sinks in the Open Ocean and in the Gulf Coast, while alkenes and biogenics were the most important NO_3 sinks in the polluted regions. The peroxy radicals accounted, on average, for 12–28% of the total gas-phase NO_3 sinks in the clean and semi-polluted regions, consistent with a previous study. In the polluted regions, the peroxy radicals accounted, on average, for 1–2% of the total gas-phase NO_3 sinks. The quantification of the NO_3 – RO_2 interactions was possible because the two parameters were measured simultaneously on the R/V *Brown* during the TexAQS 2006 cruise.

Acknowledgements We thank the crew of the NOAA R/V *Brown* for their contribution to the field work. Thanks to M.J. Pilling and C.J. Martin for assistance in setting up the MCM model and to A. Bonzanini for help in assembling the appendix. This work was funded in part by NOAA's Air Quality and Atmospheric Chemistry and Climate Programs and in part by the Texas Commission on Environmental Quality (TCEQ).

Appendix: RO_2 precursors in MCM v3.1

Peroxy radical	Precursor VOC
ISOPO2 = ISOPAO2, ISOPBO2, ISOPCO2, ISOPDO2, NISOP2	isoprene
MACRO2, MACO3	isoprene, methacrolein
HMVKAO2	isoprene, α -pinene, β -pinene, methyl vinyl ketone
HMVKBO2	isoprene, methyl vinyl ketone
APINAO2, APINBO2, APINCO2, NAPINAO2, NAPINBO2	α -pinene
BPINAO2, BPINBO2, BPINCO2, NBPINAO2, NBPINBO2	β -pinene
ALKAO2 = C2H5O2	ethane, propane, n-butane, n-pentane, i-pentane, neo-pentane, 2,2-dimethylbutane, 2,3-dimethylbutane, 2-methylpentane, 3-methylpentane, n-hexane, 2-methylhexane, 3-methylhexane, n-heptane, n-octane, n-nonane, n-decane, n-undecane, n-dodecane, cyclohexane, 1-butene, 2-methyl-1-butene,

Peroxy radical	Precursor VOC
	3-methyl-1-butene, 1-pentene, cis-2-pentene, trans-2-pentene, 1-hexene, cis-2-hexene, trans-2-hexene, ethylbenzene, n-propyl benzene, i-propyl benzene, 1-ethyl 2-methyl benzene, 1-ethyl 3-methyl benzene, 1-ethyl 4-methyl benzene, 3,5-dimethyl ethylbenzene, 3,5-diethyl toluene, propanal, butanal, pentanal, methyl ethyl ketone, methyl n-propyl ketone, methyl i-propyl ketone, diethyl ketone, methyl t-butyl ketone, 2-hexanone, 3-hexanone, cyclohexanone, 1-propanol, 1-butanol, 2-butanol, 2-methyl-1-butanol, 2-methyl-2-butanol, 3-methyl-2-butanol, 3-pentanol, cyclohexanol, diethyl ether, ethyl t-butyl ether, 2-ethoxy ethanol, 2-butoxy ethanol, 1-butoxy 2-propanol, ethyl acetate, n-propyl acetate, n-butyl acetate, s-butyl acetate, propanoic acid
NC3H7O2	propane, n-butane, n-pentane, 2-methylpentane, n-hexane, 2-methylhexane, n-heptane, n-octane, n-nonane, n-decane, n-undecane, n-dodecane, cyclohexane, 3-methyl-1-butene, 1-pentene, 1-hexene, cis-2-hexene, trans-2-hexene, n-propyl benzene, i-propyl benzene, butanal, pentanal, methyl n-propyl ketone, methyl n-butyl ketone, ethyl n-propyl ketone, cyclohexanone, 1-butanol, cyclohexanol, 2-butoxy ethanol, 1-butoxy 2-propanol, n-butyl acetate
IC3H7O2	propane, n-butane, i-butane, n-pentane, i-pentane, 2,3-dimethylbutane, 2-methylpentane, n-hexane, 2-methylhexane, 3-methylhexane, n-heptane, n-octane, n-nonane, n-decane, n-undecane, n-dodecane, cyclohexane, 3-methyl-1-butene, 1-pentene, 1-hexene, cis-2-hexene, trans-2-hexene, n-propyl benzene, i-propyl benzene, 2-methylpropanal, butanal, pentanal, methyl n-propyl ketone, methyl i-propyl ketone, methyl n-butyl ketone, methyl i-butyl ketone, ethyl n-propyl ketone, cyclohexanone, 2-methyl-1-propanol, 1-butanol, 3-methyl-1-butanol, 3-methyl-2-butanol, cyclohexanol, 2-butoxy ethanol, 1-butoxy 2-propanol, n-butyl acetate
NC4H9O2	n-butane, n-pentane, n-hexane, n-heptane, n-octane, n-nonane, n-decane, n-undecane, n-dodecane, 1-hexene, pentanal, methyl n-butyl ketone, 2-butoxy ethanol
SC4H9O2	n-butane, i-pentane, 3-methylpentane, 2-methylhexane, 3-methylhexane, 1-hexene, 2-methyl-1-butanol
IC4H9O2	i-butane, 2-methylpentane, methyl i-butyl ketone, 3-methyl-1-butanol
TC4H9O2	i-butane, 2,2-dimethylpropane, 2,2-dimethylbutane, methyl t-butyl ketone, methyl t-butyl ether, ethyl t-butyl ether, t-butyl acetate
PEAO2	n-pentane, n-hexane, n-octane, n-nonane, n-decane, n-undecane, n-dodecane
PEBO2	n-pentane, 2-methylpentane
PECO2	n-pentane
IPEAO2	i-pentane, 3-methylpentane, 2-methylhexane, 3-methylhexane
IPEBO2	i-pentane, 2,3-dimethylbutane
IPECO2	i-pentane, 2,2-dimethylbutane

Peroxy radical	Precursor VOC
ALKEO2 = HOCH2CH2O2	ethane, propane, n-butane, n-pentane, i-pentane, neo-pentane, 2,2-dimethylbutane, 2,3-dimethylbutane, 2-methylpentane, 3-methylpentane, n-hexane, 2-methylhexane, 3-methylhexane, n-heptane, n-octane, n-nonane, n-decane, n-undecane, n-dodecane, cyclohexane, ethene, 1-butene, 2-methyl-1-butene, 3-methyl-1-butene, 1-pentene, cis-2-pentene, trans-2-pentene, 1-hexene, cis-2-hexene, trans-2-hexene, 1,3-butadiene, α -pinene, β -pinene, ethylbenzene, n-propyl benzene, i-propyl benzene, 1-ethyl 2-methyl benzene, 1-ethyl 3-methyl benzene, 1-ethyl 4-methyl benzene, 3,5-dimethyl ethylbenzene, 3,5-diethyl toluene, propanal, butanal, pentanal, methyl ethyl ketone, methyl n-propyl ketone, methyl i-propyl ketone, diethyl ketone, methyl n-butyl ketone, methyl t-butyl ketone, ethyl n-propyl ketone, cyclohexanone, ethanol, 1-propanol, 1-butanol, 2-butanol, 2-methyl-1-butanol, 2-methyl-2-butanol, 3-methyl-1-butanol, 3-methyl-2-butanol, 3-pentanol, cyclohexanol, diethyl ether, ethyl t-butyl ether, 2-ethoxy ethanol, 2-butoxy ethanol, 1-butoxy 2-propanol, ethyl acetate, n-propyl acetate, n-butyl acetate, s-butyl acetate, propanoic acid
ETHENO3O2	n-butane, n-pentane, n-hexane, 2-methylhexane, n-heptane, n-octane, n-nonane, n-decane, n-undecane, n-dodecane, cyclohexane, ethene, 1-pentene, 1-hexene, cis-2-hexene, trans-2-hexene, 1,3-butadiene, n-propyl benzene, i-propyl benzene, butanal, pentanal, methyl n-butyl ketone, cyclohexanone, 1-butanol, cyclohexanol, 2-butoxy ethanol, 1-butoxy 2-propanol, n-butyl acetate
HYPROPO2	propane, n-butane, i-butane, n-pentane, i-pentane, 2,2-dimethylbutane, 2,3-dimethylbutane, 2-methylpentane, 3-methylpentane, n-hexane, 2-methylhexane, 3-methylhexane, n-heptane, n-octane, n-nonane, n-decane, n-undecane, n-dodecane, cyclohexane, propene, 3-methyl-1-butene, 1-pentene, 1-hexene, cis-2-hexene, trans-2-hexene, isoprene, n-propyl benzene, i-propyl benzene, 2-methylpropanal, butanal, pentanal, methyl n-propyl ketone, methyl i-propyl ketone, methyl n-butyl ketone, methyl i-butyl ketone, methyl t-butyl ketone, ethyl n-propyl ketone, cyclohexanone, 1-propanol, 2-methyl-1-propanol, 1-butanol, 2-methyl-1-butanol, 3-methyl-1-butanol, 3-methyl-2-butanol, cyclohexanol, 2-butoxy ethanol, 1-butoxy 2-propanol, n-butyl acetate
IPROPULO2	propane, n-butane, i-butane, n-pentane, i-pentane, 2,3-dimethylbutane, 2-methylpentane, 3-methylpentane, n-hexane, 2-methylhexane, 3-methylhexane, n-heptane, n-octane, n-nonane, n-decane, n-undecane, n-dodecane, cyclohexane, propene, 3-methyl-1-butene, 1-pentene, 1-hexene, cis-2-hexene, trans-2-hexene, isoprene, n-propyl benzene, i-propyl benzene, 2-methylpropanal, butanal, pentanal, methyl n-propyl ketone, methyl i-propyl ketone, methyl n-butyl ketone, methyl i-butyl ketone, ethyl n-propyl ketone, cyclohexanone, 2-propanol, 2-methyl-1-propanol, 1-butanol, 2-methyl-1-butanol, 3-methyl-1-butanol, 3-methyl-2-butanol, cyclohexanol, 2-methyl-3-buten-2-ol (MBO), 2-butoxy ethanol, 1-butoxy 2-propanol, n-butyl acetate

Peroxy radical	Precursor VOC
PRONO3AO2, PRONO3BO2	i-pentane, 3-methylpentane, 2-methylhexane, 3-methylhexane, cyclohexane, propene, isoprene, cyclohexanone, 2-methyl-1-butanol, cyclohexanol
NBUTOLAO2	n-butane, n-pentane, n-hexane, n-heptane, n-octane, n-nonane, n-decane, n-undecane, n-dodecane, 1-butene, 1-hexene, pentanal, methyl n-butyl ketone, 1-butanol, 2-butoxy ethanol
HO3C4O2	n-pentane, n-hexane, n-heptane, n-octane, n-nonane, n-decane, n-undecane, n-dodecane, 1-butene, 1-hexene, pentanal, methyl n-butyl ketone, 3-pentanol
BU1ENO3O2, C43NO34O2	n-hexane, n-nonane, n-decane, n-undecane, n-dodecane, 1-butene
BUT2OLO2	n-butane, i-pentane, 2,3-dimethylbutane, 3-methylpentane, 2-methylhexane, 3-methylhexane, cis-2-butene, trans-2-butene, 1-hexene, 2-butanol, 2-methyl-1-butanol, 3-methyl-2-butanol
C42NO33O2	cis-2-butene, trans-2-butene
IBUTOLBO2	i-butane, 2,2-dimethylbutane, 2-methylpentane, methylpropene, methyl i-butyl ketone, methyl t-butyl ketone, 2-methyl-1-propanol, 3-methyl-1-butanol
TBUTOLO2	i-butane, i-pentane, neo-pentane, 2,2-dimethylbutane, 2-methylpentane, 2-methylhexane, methylpropene, β -pinene, methyl i-butyl ketone, methyl t-butyl ketone, 2-methyl-2-propanol, 2-methyl-2-butanol, 3-methyl-1-butanol, diacetone alcohol, methyl t-butyl ether, ethyl t-butyl ether, t-butyl acetate
MPRANO3O2	methylpropene
MPRBNO3O2	methylpropene, 3-methyl-1-butanol
BU1ENO3O2	n-hexane, n-nonane, n-decane, n-undecane, n-dodecane, 1-butene
PE1ENEA02, C51NO32O2	cyclohexane, 1-pentene, cyclohexanone, cyclohexanol
PE1ENEBO2	n-octane, n-undecane, cyclohexane, 1-pentene, cyclohexanone, cyclohexanol
C52NO31O2	cyclohexane, 1-pentene, cyclohexanone, cyclohexanol
PE2ENEA02, C52NO33O2, C53NO32O2	cis-2-pentene, trans-2-pentene
PE2ENEBO2	n-pentane, cis-2-pentene, trans-2-pentene, 3-pentanol
M2BUOL2O2	i-pentane, 3-methylpentane, 2-methylhexane, 3-methylhexane, 2-methyl-1-butene, 2-methyl-1-butanol
PROL11MO2	i-pentane, 2,2-dimethylbutane, 3-methylhexane, 2-methyl-1-butene, 2-methyl-2-butanol
C4NO32M1O2, C4NO32M2O2	2-methyl-1-butene
ME3BUOLO2	3-methyl-1-butene, 3-methyl-1-butanol
ME3BU2OLO2	2-methylhexane, 3-methyl-1-butene
C4M3NO31O2, C4M3NO32O2	3-methyl-1-butene
BUTDAO2, BUTDBO2, BUTDCO2, NBUTDAO2, NBUTDBO2	1,3-butadiene

Peroxy radical	Precursor VOC
CARBO2 = CH ₃ CO ₃	ethane, propane, n-butane, i-butane, n-pentane, i-pentane, neo-pentane, 2,2-dimethylbutane, 2,3-dimethylbutane, 2-methylpentane, 3-methylpentane, n-hexane, 2-methylhexane, 3-methylhexane, n-heptane, n-octane, n-nonane, n-decane, n-undecane, n-dodecane, cyclohexane, propene, 1-butene, cis-2-butene, trans-2-butene, methylpropene, 2-methyl-1-butene, 2-methyl-2-butene, 3-methyl-1-butene, 1-pentene, cis-2-pentene, trans-2-pentene, 1-hexene, cis-2-hexene, trans-2-hexene, 2,3-dimethyl but-2-ene, isoprene, α -pinene, β -pinene, toluene, o-xylene, m-xylene, p-xylene, ethylbenzene, n-propyl benzene, i-propyl benzene, 1,2,3-trimethyl benzene, 1,2,4-trimethyl benzene, 1,3,5-trimethyl benzene, 1-ethyl 2-methyl benzene, 1-ethyl 3-methyl benzene, 1-ethyl 4-methyl benzene, 3,5-dimethyl ethylbenzene, 3,5-diethyl toluene, acetaldehyde, propanal, 2-methylpropanal, butanal, pentanal, acetone, methyl ethyl ketone, methyl n-propyl ketone, methyl i-propyl ketone, diethyl ketone, methyl i-butyl ketone, methyl t-butyl ketone, 2-hexanone, 3-hexanone, cyclohexanone, ethanol, 1-propanol, 2-propanol, 2-methyl-1-propanol, 2-methyl-2-propanol, 1-butanol, 2-butanol, 2-methyl-1-butanol, 2-methyl-2-butanol, 3-methyl-1-butanol, 3-methyl-2-butanol, 3-pentanol, cyclohexanol, diacetone alcohol, 2-methyl-3-buten-2-ol (MBO), propylene glycol, methyl t-butyl ether, diethyl ether, ethyl t-butyl ether, di i-propyl ether, 2-ethoxy ethanol, 2-butoxy ethanol, 1-butoxy 2-propanol, 1-methoxy 2-propanol, methyl acetate, ethyl acetate, n-propyl acetate, i-propyl acetate, n-butyl acetate, s-butyl acetate, t-butyl acetate, propanoic acid, chloroethane, 1,1-dichloroethane, 1,2-dichloropropane
C ₂ H ₅ CO ₃	propane, n-butane, n-pentane, i-pentane, 2,2-dimethylbutane, 2,3-dimethylbutane, 2-methylpentane, 3-methylpentane, n-hexane, 2-methylhexane, 3-methylhexane, n-heptane, n-octane, n-nonane, n-decane, n-undecane, n-dodecane, cyclohexane, 1-butene, 2-methyl-1-butene, 3-methyl-1-butene, 1-pentene, cis-2-pentene, trans-2-pentene, 1-hexene, cis-2-hexene, trans-2-hexene, ethylbenzene, n-propyl benzene, i-propyl benzene, 1-ethyl 2-methyl benzene, 1-ethyl 3-methyl benzene, 1-ethyl 4-methyl benzene, 3,5-dimethyl ethylbenzene, 3,5-diethyl toluene, propanal, butanal, pentanal, methyl ethyl ketone, methyl n-propyl ketone, methyl i-propyl ketone, diethyl ketone, methyl t-butyl ketone, 2-hexanone, 3-hexanone, cyclohexanone, 1-propanol, 1-butanol, 2-butanol, 2-methyl-1-butanol, 2-methyl-2-butanol, 3-methyl-2-butanol, 3-pentanol, cyclohexanol, 2-butoxy ethanol, 1-butoxy 2-propanol, n-propyl acetate, n-butyl acetate, s-butyl acetate
CH ₃ COCH ₂ O ₂	propane, n-butane, i-butane, n-pentane, i-pentane, neo-pentane, 2,2-dimethylbutane, 2,3-dimethylbutane, 2-methylpentane, 3-methylpentane, n-hexane, 2-methylhexane, 3-methylhexane, n-heptane, n-octane, n-nonane, n-decane, n-undecane, n-dodecane, cyclohexane, methylpropene, 2-methyl-1-butene,

Peroxy radical	Precursor VOC
	2-methyl-2-butene, 3-methyl-1-butene, 1-pentene, 1-hexene, cis-2-hexene, trans-2-hexene, 2,3-dimethyl but-2-ene, α -pinene, β -pinene, o-xylene, n-propyl benzene, i-propyl benzene, 1,2,3-trimethyl benzene, 1,2,4-trimethyl benzene, 3,5-diethyl toluene, 2-methylpropanal, butanal, pentanal, acetone, methyl ethyl ketone, methyl n-propyl ketone, methyl i-propyl ketone, methyl n-butyl ketone, methyl i-butyl ketone, methyl t-butyl ketone, ethyl n-propyl ketone, cyclohexanone, 2-propanol, 2-methyl-1-propanol, 2-methyl-2-propanol, 1-butanol, 2-butanol, 2-methyl-1-butanol, 2-methyl-2-butanol, 3-methyl-1-butanol, 3-methyl-2-butanol, cyclohexanol, diacetone alcohol, 2-methyl-3-buten-2-ol (MBO), methyl t-butyl ether, ethyl t-butyl ether, di i-propyl ether, 2-butoxy ethanol, 1-butoxy 2-propanol, i-propyl acetate, n-butyl acetate, s-butyl acetate, t-butyl acetate
MEKAO2	n-butane, n-pentane, i-pentane, 2,2-dimethylbutane, 2-methylpentane, 3-methylpentane, n-hexane, 2-methylhexane, 3-methylhexane, n-heptane, n-octane, n-nonane, n-decane, n-undecane, n-dodecane, cyclohexane, 2-methyl-1-butene, 1-hexene, methyl ethyl ketone, methyl n-butyl ketone, 2-butanol, 2-methyl-1-butanol, 2-methyl-2-butanol, cyclohexanol, s-butyl acetate
MEKBO2	n-butane, i-pentane, 2,2-dimethylbutane, 2,3-dimethylbutane, 3-methylpentane, 2-methylhexane, 3-methylhexane, 2-methyl-1-butene, 1-hexene, o-xylene, 1,2,3-trimethyl benzene, 1,2,4-trimethyl benzene, methyl ethyl ketone, methyl i-propyl ketone, methyl t-butyl ketone, 2-butanol, 2-methyl-1-butanol, 2-methyl-2-butanol, 3-methyl-2-butanol, s-butyl acetate
MEKCO2	n-butane, n-pentane, i-pentane, 2,2-dimethyl butane, 3-methylpentane, n-hexane, 2-methylhexane, 3-methylhexane, n-heptane, n-octane, n-nonane, n-decane, n-undecane, n-dodecane, 2-methyl-1-butene, 1-hexene, 3,5-diethyl toluene, pentanal, methyl ethyl ketone, diethyl ketone, methyl n-butyl ketone, ethyl n-propyl ketone, 2-butanol, 2-methyl-1-butanol, 2-methyl-2-butanol, 3-pentanol, s-butyl acetate
AROM2 =	
BZBIPERO2	benzene
C6H5CH2O2	toluene, ethylbenzene
TLBIPERO2	toluene
OXYBIPERO2, OXYLO2	o-xylene
MXYBIPERO2, MXYLO2	m-xylene
PXYBIPERO2, PXYLO2	p-xylene
C6H5C2H4O2, EBZBIPERO2	ethylbenzene
STYRENO2, NSTYRENO2	styrene

References

- Aldener, M., Brown, S.S., Stark, H., Williams, E.J., Lerner, B.M., Kuster, W.C., Goldan, P.D., Quinn, P.K., Bates, T.S., Fehsenfeld, F.C., Ravishankara, A.R.: Reactivity and loss mechanisms of NO_3 and N_2O_5 in a polluted marine environment: results from in situ measurements during New England Air Quality Study 2002. *J. Geophys. Res.* **111**, D23S73 (2006). doi:[10.1029/2006JD007252](https://doi.org/10.1029/2006JD007252)
- Ambrose, J.L., Mao, H., Mayne, H.R., Stutz, J., Talbot, R., Sive, B.C.: Nighttime nitrate radical chemistry at Appledore Island, Maine during the 2004 International Consortium for Atmospheric Research on Transport and Transformation. *J. Geophys. Res.* **112**, D21302 (2007). doi:[10.1029/2007JD008756](https://doi.org/10.1029/2007JD008756)
- Atkinson, R., Cox, R.A., Crowley, J.N., Hampson, R.F., Hynes, R.G., Jenkin, M.E., Kerr, J.A., Rossi, M.J., Troe, J.: Summary of evaluated kinetic and photochemical data for atmospheric chemistry. Tech. rep., IUPAC Subcommittee on Gas Kinetic Data Evaluation for Atmospheric Chemistry (2006). <http://www.iupac-kinetic.ch.cam.ac.uk/>
- Bates, T.S., Quinn, P.K., Coffman, D., Schulz, K., Covert, D.S., Johnson, J.E., Williams, E.J., Lerner, B.M., Angevine, W.M., Tucker, S.C., Brewer, W.A., Stohl, A.: Boundary layer aerosol chemistry during TexAQS/GoMACCS 2006; insights into aerosol sources and transformation processes. *J. Geophys. Res.* **113**, D00F01 (2008). doi:[10.1029/2008JD010023](https://doi.org/10.1029/2008JD010023)
- Brown, S.S., Ryerson, T.B., Wollny, A.G., Brock, C.A., Peltier, R., Sullivan, A.P., Weber, R.J., Holloway, J.S., Dubé, W.P., Trainer, M., Meagher, J.F., Fehsenfeld, F.C., Ravishankara, A.R.: Variability in nocturnal nitrogen oxide processing and its role in regional air quality. *Science* **311**, 67–70 (2006)
- Brown, S.S., de Gouw, J.A., Warneke, C., Ryerson, T.B., Dubé, W.P., Atlas, E., Weber, R.J., Peltier, R.E., Neuman, J.A., Roberts, J.M., Swanson, A., Flocke, F., McKeen, S.A., Brioude, J., Sommariva, R., Trainer, M., Fehsenfeld, F.C., Ravishankara, A.R.: Nocturnal isoprene oxidation over the Northeast United States in summer and its impact on reactive nitrogen partitioning and secondary organic aerosol. *Atmos. Chem. Phys.* **9**(9), 3027–3042 (2009). www.atmos-chem-phys.net/9/3027/2009/
- Brown, S.S., Dubé, W.P., Peischl, J., Ryerson, T.B., Atlas, E., Warneke, C., de Gouw, J.A., te Lintel Hekkert, S., Brock, C.A., Flocke, F., Trainer, M., Parrish, D.D., Fehsenfeld, F.C., Ravishankara, A.R.: Budgets for nocturnal VOC oxidation by nitrate radicals aloft during the 2006 Texas Air Quality Study. *J. Geophys. Res.* **116**, D24305 (2011). doi:[10.1029/2011JD016544](https://doi.org/10.1029/2011JD016544)
- Canosa-Mas, C.E., King, M.D., Lopez, R., Percival, C.J., Wayne, R.P., Shallcross, D.E., Pyle, J.A., Daële, V.: Is the reaction between $\text{CH}_3\text{C}(\text{O})\text{O}_2$ and NO_3 important in the night-time troposphere? *Faraday Trans.* **92**, 2211–2222 (1996). doi:[10.1039/FT9969202211](https://doi.org/10.1039/FT9969202211)
- Carslaw, N., Carpenter, L.J., Plane, J.M.C., Allan, B.J., Burgess, R.A., Clemitshaw, K.C., Coe, H., Penkett, S.A.: Simultaneous observations of nitrate and peroxy radicals in the marine boundary layer. *J. Geophys. Res.* **102**(D15), 18,917–18,933 (1997)
- Carslaw, N., Creasey, D.J., Heard, D.E., Lewis, A.C., McQuaid, J.B., Pilling, M.J., Monks, P.S., Bandy, B.J., Penkett, S.A.: Modeling OH, HO_2 , and RO_2 radicals in the marine boundary layer—1. Model construction and comparison with field measurements. *J. Geophys. Res.* **104**(D23), 30,241–30,255 (1999)
- Carslaw, N., Creasey, D.J., Heard, D.E., Jacobs, P.J., Lee, J.D., Lewis, A.C., McQuaid, J.B., Pilling, M.J., Bauguutte, S., Penkett, S.A., Monks, P.S., Salisbury, G.: Eastern Atlantic Spring Experiment 1997 (EASE97)—2. Comparisons of model concentrations of OH, HO_2 , and RO_2 with measurements. *J. Geophys. Res.* **107**(D14), 4190 (2002). doi:[10.1029/2001JD001568](https://doi.org/10.1029/2001JD001568)
- Dubé, W.P., Brown, S.S., Osthoff, H.D., Nunley, M.R., Ciciora, S.J., Paris, M.W., McLaughlin, R.J., Ravishankara, A.R.: Aircraft instrument for simultaneous, in situ measurement of NO_3 and N_2O_5 via pulsed cavity ring-down spectroscopy. *Rev. Sci. Instrum.* **77**, 034101 (2006)
- Emmerson, K.M., Carslaw, N., Carslaw, D.C., Lee, J.D., McFiggans, G., Bloss, W.J., Gravestock, T., Heard, D.E., Hopkins, J., Ingham, T., Pilling, M.J., Smith, S.C., Jacob, M., Monks, P.S.: Free radical modelling studies during the UK TORCH campaign in summer 2003. *Atmos. Chem. Phys.* **7**, 167–181 (2007)
- Fleming, Z.L., Monks, P.S., Rickard, A.R., Heard, D.E., Bloss, W.J., Seakins, P.W., Still, T.J., Sommariva, R., Pilling, M.J., Morgan, R., Green, T.J., Brough, N., Mills, G.P., Penkett, S.A., Lewis, A.C., Lee, J.D., Saiz-Lopez, A., Plane, J.M.C.: Peroxy radical chemistry and the control of ozone photochemistry at Mace Head, Ireland during the summer of 2002. *Atmos. Chem. Phys.* **6**(8), 2193–2214 (2006) www.atmos-chem-phys.net/6/2193/2006/

- Fuchs, H., Bohn, B., Hofzumahaus, A., Holland, F., Lu, K.D., Nehr, S., Rohrer, F., Wahner, A.: Detection of HO₂ by laser-induced fluorescence: calibration and interferences from RO₂ radicals. *Atmos. Meas. Tech.* **4**, 1209–1225 (2011)
- Fuchs, N.A., Sutugin, A.G.: *Highly Dispersed Aerosols*. Ann Arbor Science, Ann Arbor, MI, USA (1970)
- Geyer, A., Bächmann, K., Hofzumahaus, A., Holland, F., Konrad, S., Klüpfel, T., Pätz, H.W., Perner, D., Mihelcic, D., Schäfer, H.J., Volz-Thomas, A., Platt, U.: Nighttime formation of peroxy and hydroxyl radicals during the BERLIOZ campaign: observations and modeling studies. *J. Geophys. Res.* **108**(D4), 8249 (2003). doi:[10.1029/2001JD000656](https://doi.org/10.1029/2001JD000656)
- Gilman, J.B., Kuster, W.C., Goldan, P.D., Herndon, S.C., Zahniser, M.S., Tucker, S.C., Brewer, W.A., Lerner, B.M., Williams, E.J., Harley, R.A., Fehsenfeld, F.C., Warneke, C., de Gouw, J.A.: Measurements of volatile organic compounds during the 2006 TexAQ/GoMACCS campaign: industrial influences, regional characteristics, and diurnal dependencies of the OH reactivity. *J. Geophys. Res.* **114**, D00F06 (2009). doi:[10.1029/2008JD011525](https://doi.org/10.1029/2008JD011525)
- Jenkin, M.E., Saunders, S.M., Pilling, M.J.: The tropospheric degradation of volatile organic compounds: a protocol for mechanism development. *Atmos. Environ.* **31**(1), 81–104 (1997)
- Jenkin, M.E., Saunders, S.M., Wagner, V., Pilling, M.J.: Protocol for the development of the Master Chemical Mechanism, MCM v3 (Part B): tropospheric degradation of aromatic volatile organic compounds. *Atmos. Chem. Phys.* **3**(1), 181–193 (2003)
- Kirchner, F., Mayer-Figge, A., Zabel, F., Becker, K.H.: Thermal stability of peroxy nitrates. *Int. J. Chem. Kinet.* **31**, 127–144 (1999)
- Kuster, W.C., Jobson, B.T., Karl, T., Riemer, D., Apel, E., Goldan, P.D., Fehsenfeld, F.C.: Intercomparison of volatile organic carbon measurement techniques and data at La Porte during the TexAQ/2000 Air Quality Study. *Environ. Sci. Technol.* **38**, 221–228 (2004)
- Mentel, T.F., Bleilebens, D., Wahner, A.: A study of nighttime nitrogen oxide oxidation in a large reaction chamber—the fate of NO₂, N₂O₅, HNO₃, and O₃ at different humidities. *Atmos. Environ.* **30**(23), 4007–4020 (1996)
- Mihelcic, D., Klemp, D., Müsgen, P., Pätz, H.W., Volz-Thomas, A.: Simultaneous measurements of peroxy and nitrate radicals at Schauinsland. *J. Atmos. Chem.* **16**, 313–335 (1993)
- Monks, P.S.: Gas-phase radical chemistry in the troposphere. *Chem. Soc. Rev.* **34**, 376–395 (2005)
- Osthoff, H.D., Sommariva, R., Baynard, T., Pettersson, A., Williams, E.J., Lerner, B.M., Roberts, J.M., Stark, H., Goldan, P.D., Kuster, W.C., Bates, T.S., Coffman, D., Ravishankara, A.R., Brown, S.S.: Observation of daytime N₂O₅ in the marine boundary layer during New England Air Quality Study-Intercontinental Transport and Chemical Transformation 2004. *J. Geophys. Res.* **111**, D23S14 (2006). doi:[10.1029/2006JD007593](https://doi.org/10.1029/2006JD007593)
- Osthoff, H.D., Roberts, J.M., Ravishankara, A.R., Williams, E.J., Lerner, B.M., Sommariva, R., Bates, T.S., Coffman, D., Quinn, P.K., Dibb, J.E., Stark, H., Burkholder, J.B., Talukdar, R.K., Meagher, J., Fehsenfeld, F.C., Brown, S.S.: High levels of nitryl chloride in the polluted subtropical marine boundary layer. *Nature Geosci.* **1**, 324–328 (2008). doi:[10.1038/ngeo177](https://doi.org/10.1038/ngeo177)
- Osthoff, H.D., Bates, T.S., Johnson, J.E., Kuster, W.C., Goldan, P.D., Sommariva, R., Williams, E.J., Lerner, B.M., Warneke, C., de Gouw, J.A., Pettersson, A., Baynard, T., Meagher, J.F., Fehsenfeld, F.C., Ravishankara, A.R., Brown, S.S.: Regional variation of the dimethyl sulfide oxidation mechanism in the summertime marine boundary layer in the Gulf of Maine. *J. Geophys. Res.* **114**, D07301 (2009). doi:[10.1029/2008JD010990](https://doi.org/10.1029/2008JD010990)
- Parrish, D.D., Allen, D.T., Bates, T.S., Estes, M., Fehsenfeld, F.C., Feingold, G., Ferrare, R., Hardesty, R.M., Meagher, J.F., Nielsen-Gammon, J.W., Pierce, R.B., Ryerson, T.B., Seinfeld, J.H., Williams, E.J.: Overview of the Second Texas Air Quality Study (TexAQ/II) and the Gulf of Mexico Atmospheric Composition and Climate Study (GoMACCS). *J. Geophys. Res.* **114**, D00F13 (2009). doi:[10.1029/2009JD011842](https://doi.org/10.1029/2009JD011842)
- Roberts, J.M., Jobson, B.T., Kuster, W.C., Goldan, P.D., Murphy, P., Williams, E., Frost, G., Riemer, D., Apel, E., Stroud, C., Wiedinmyer, C., Fehsenfeld, F.C.: An examination of the chemistry of peroxy-carboxylic nitric anhydrides and related volatile organic compounds during Texas Air Quality Study 2000 using ground-based measurements. *J. Geophys. Res.* **108**(D16), 4495 (2003). doi:[10.1029/2003JD003383](https://doi.org/10.1029/2003JD003383)
- Salisbury, G., Rickard, A.R., Monks, P.S., Allan, B.J., Bauguitte, S., Penkett, S.A., Carslaw, N., Lewis, A.C., Creasey, D.J., Heard, D.E., Jacobs, P.J., Lee, J.D.: Production of peroxy radicals at night via reactions of ozone and the nitrate radical in the marine boundary layer. *J. Geophys. Res.* **106**(D12), 12,669–12,687 (2001)
- Saunders, S.M., Jenkin, M.E., Derwent, R.G., Pilling, M.J.: Protocol for the development of the Master Chemical Mechanism, MCM v3 (Part A): tropospheric degradation of non-aromatic volatile organic compounds. *Atmos. Chem. Phys.* **3**(1), 161–180 (2003)

- Seefeld, S., Kerr, J.A.: Kinetics of the reactions of propionylperoxy radicals with NO and NO₂: peroxypropionyl nitrate formation under laboratory conditions related to the troposphere. *Environ. Sci. Technol.* **31**, 2949–2953 (1997)
- Sommariva, R., Haggerstone, A.L., Carpenter, L.J., Carslaw, N., Creasey, D.J., Heard, D.E., Lee, J.D., Lewis, A.C., Pilling, M.J., Zádor, J.: OH and HO₂ chemistry in clean marine air during SOAPEX-2. *Atmos. Chem. Phys.* **4**(3), 839–856 (2004). www.atmos-chem-phys.net/4/839/2004/
- Sommariva, R., Bloss, W.J., Brough, N., Carslaw, N., Flynn, M., Haggerstone, A.L., Heard, D.E., Hopkins, J.R., Lee, J.D., Lewis, A.C., McFiggans, G., Monks, P.S., Penkett, S.A., Pilling, M.J., Plane, J.M.C., Read, K.A., Saiz-Lopez, A., Rickard, A.R., Williams, P.I.: OH and HO₂ chemistry during NAMBLEX: roles of oxygenates, halogen oxides and heterogeneous uptake. *Atmos. Chem. Phys.* **6**(4), 1135–1153 (2006). www.atmos-chem-phys.net/6/1135/2006/
- Sommariva, R., Trainer, M., de Gouw, J.A., Roberts, J.M., Warneke, C., Atlas, E., Flocke, F., Goldan, P.D., Kuster, W.C., Swanson, A.L., Fehsenfeld, F.C.: A study of organic nitrates formation in an urban plume using a Master Chemical Mechanism. *Atmos. Environ.* **42**(23), 5771–5786 (2008). doi:10.1016/j.atmosenv.2007.12.031
- Sommariva, R., Osthoff, H.D., Brown, S.S., Bates, T.S., Baynard, T., Coffman, D., de Gouw, J.A., Goldan, P.D., Kuster, W.C., Lerner, B.M., Stark, H., Warneke, C., Williams, E.J., Fehsenfeld, F.C., Ravishankara, A.R., Trainer, M.: Radicals in the marine boundary layer during NEAQS 2004: a model study of day-time and night-time sources and sinks. *Atmos. Chem. Phys.* **9**(9), 3075–3093 (2009). www.atmos-chem-phys.net/9/3075/2009/
- Sommariva, R., Brown, S.S., Roberts, J.M., Brookes, D.M., Parker, A.E., Monks, P.S., Bates, T.S., Bon, D., de Gouw, J.A., Frost, G.J., Gilman, J.B., Goldan, P.D., Herndon, S.C., Kuster, W.C., Lerner, B.M., Osthoff, H.D., Tucker, S.C., Warneke, C., Williams, E.J., Zahniser, M.S.: Ozone production in remote oceanic and industrial areas derived from ship based measurements of peroxy radicals during TexAQS 2006. *Atmos. Chem. Phys.* **11**(6), 2471–2485 (2011). www.atmos-chem-phys.net/11/2471/2011/
- Stutz, J., Wong, K.W., Lawrence, L., Ziemba, L., Flynn, J.H., Rappenglück, B., Lefer, B.: Nocturnal NO₃ radical chemistry in Houston, TX. *Atmos. Environ.* **44**(33), 4099–4106 (2010)
- Taketani, F., Kanaya, Y., Akimoto, H.: Kinetics of heterogeneous reactions of HO₂ radical at ambient concentration levels with (NH₄)₂SO₄ and NaCl aerosol particles. *J. Phys. Chem., A* **112**(11), 2370–2377 (2008)
- Taketani, F., Kanaya, Y., Akimoto, H.: Heterogeneous loss of HO₂ by KCl, synthetic sea salt and natural seawater aerosol particles. *Atmos. Environ.* **43** 1660–1665 (2009)
- Thornton, J., Abbatt, J.P.D.: Measurements of HO₂ uptake to aqueous aerosol: mass accommodation coefficients and net reactive loss. *J. Geophys. Res.* **110**, D08309 (2005). doi:10.1029/2004JD005402
- Thornton, J.A., Jaeglé, L., McNeill, V.F.: Assessing known pathways for HO₂ loss in aqueous atmospheric aerosols: regional and global impacts on tropospheric oxidants. *J. Geophys. Res.* **113**, D05303 (2008). doi:10.1029/2007JD009236
- Tucker, S.C., Banta, R.M., Langford, A.O., Senff, C.J., Brewer, W.A., Williams, E.J., Lerner, B.M., Osthoff, H., Hardesty, R.M.: Relationships of coastal nocturnal boundary layer winds and turbulence to Houston ozone concentrations during TexAQS 2006. *J. Geophys. Res.* **115**, D10304 (2010). doi:10.1029/2009JD013169
- Vaughan, S., Canosa-Mas, C.E., Pfrang, C., Shallcross, D.E., Watson, L., Wayne, R.P.: Kinetic studies of reactions of the nitrate radical (NO₃) with peroxy radicals (RO₂): an indirect source of OH at night? *Phys. Chem. Chem. Phys.* **8**, 3749–3760 (2006)
- Wahner, A., Mentel, T.F., Sohn, M.: Gas-phase reaction of N₂O₅ with water vapor: importance of heterogeneous hydrolysis of N₂O₅ and surface desorption of HNO₃ in a large teflon chamber. *Geophys. Res. Lett.* **25**(12):2169–2172 (1998)
- Warneke, C., de Gouw, J.A., Negro, L.D., Brioude, J., McKeen, S., Stark, H., Kuster, W.C., Goldan, P.D., Trainer, M., Fehsenfeld, F.C., Wiedinmyer, C., Guenther, A.B., Hansel, A., Wisthaler, A., Atlas, E., Holloway, J.S., Ryerson, T.B., Peischl, J., Huey, L.G., Hanks, A.T.C.: Biogenic emission measurement and inventories determination of biogenic emissions in the eastern United States and Texas and comparison with biogenic emission inventories. *J. Geophys. Res.* **115**, D00F18 (2010). doi:10.1029/2009JD012445
- Whalley, L.K., Furneaux, K.L., Goddard, A., Lee, J.D., Mahajan, A., Oetjen, H., Read, K.A., Kaaden, N., Carpenter, L.J., Lewis, A.C., Plane, J.M.C., Saltzman, E.S., Wiedensohler, A., Heard, D.E.: The chemistry of OH and HO₂ radicals in the boundary layer over the tropical Atlantic Ocean. *Atmos. Chem. Phys.* **10**, 1555–1576 (2010)